Crustal velocity structure of the northern Yukon–Tanana upland, central Alaska: Results from TACT refraction/wide-angle reflection data

BRUCE C. BEAUDOIN *U.S. Geological Survey, Menlo Park, California,* and *Department of Geophysics, Stanford University, Stanford, California 94305-2215*

GARY S. FUIS
WILLIAM J. LUTTER
WALTER D. MOONEY
THOMAS E. MOORE
U.S. Geological Survey, Menlo Park, California 94025

ABSTRACT

The Fairbanks North seismic refraction/wide-angle reflection profile, collected by the U.S. Geological Survey Trans-Alaska Crustal Transect (TACT) project in 1987, crosses the complex region between the Yukon-Tanana and Ruby terranes in interior Alaska. This region is occupied by numerous small terranes elongated in a northeast-southwest direction. These seismic data reveal a crustal velocity structure that is divided into three upper-crustal and at least two middle- to lower-crustal domains. The upper-crustal domains are delineated by two steeply dipping low-velocity anomalies that are interpreted as signatures of the Victoria Creek fault, and the Beaver Creek fault or a fault buried by the Beaver Creek fault. This tripartite upper crust extends to 8–10 km depth where a subhorizontal interface undercuts the northern and central domains. Beneath the northern domain, this interface is interpreted as the southeastwardly dipping boundary between the Tozitna and Ruby terranes. The continuation of this interface beneath the central domain suggests that it may represent the detachment or basal thrust for thin-skinned tectonic amalgamation of the terranes caught between the Yukon-Tanana and Ruby terranes. The lower crust and Moho reflection exhibit differences from north to south that define at least two lower-crustal domains, interpreted as the Yukon-Tanana and Ruby terranes. Finally, the crustal thickness along the profile is nearly uniform and ranges from 31 to 34 km. Our data suggest that after initial thin-skinned amalgamation of the various terranes, this region experienced thick-skinned tectonic reorganization via strike-slip faulting. This interpretation supports a model in which at least one strand of the Tintina fault exists in this important region of Alaska.

INTRODUCTION

The tectonic history of interior Alaska is complicated and its interpretation controversial. Many authors have proposed that the multitude of interior-Alaska terranes were assembled by accretionary processes (Churkin and others, 1982; Coney and Jones, 1985; Jones and others, 1986). More recently, Dover (1990) and Weber (1990) questioned the accretionary model for a large portion of interior Alaska and instead suggested that the interior-Alaska terranes are dispersed and translated fragments of North American continental crust. Both of these general models call for a confluence of largely southward-moving terranes of arctic Alaska with largely northward-moving terranes of central and southern Alaska. This region includes the especially complicated crust separating the Yukon-Tanana terrane from the Ruby terrane (Fig. 1). Caught between these two large terranes or continental fragments are numerous smaller terranes or blocks representing different facies of continental-margin and oceanic crust. In addition, one or more splays of the Tintina fault may cut through these smaller terranes, further complicating the geology. This area exhibits many unresolved questions that are difficult to address due to poor exposure of local geology. Critical to our understanding of the tectonic history of interior Alaska is the geometry of these terranes at depth. This paper presents results from a seismic refraction/wide-angle reflection survey, hereafter referred to as the Fairbanks North profile, that provides new information on the crustal structure of these poorly exposed terranes in this critical region between the Yukon-Tanana and Ruby terranes (Fig. 1).

The present-day geometry of the terranes crossed by the Fairbanks North profile is ambiguous and variously interpreted. Interpretations indicate the Tintina and related faults played a major role in the development of the region. The Tintina fault is a major northwest-trending strike-slip fault of the Canadian Cordillera that extends northwestward into east-central Alaska. Along much of its length, it is exposed as a linear trench filled with Upper Cretaceous and lower Tertiary sedimentary rocks. About 450 km of right-slip displacement since Cretaceous time has been documented (Roddick, 1967; Tempelman-Kluit, 1976; Gordey, 1981), but as much as 1,000 km of total slip has been proposed for the Canadian segment (Gabrielse, 1985). East of the Fairbanks North profile, the Tintina fault consists of two subparallel strands, the Hot Springs and northern Preacher strands (Foster and others, 1983) (Fig. 1), with displacements as young as Eocene.

It is unclear whether the Tintina fault extends into the part of interior Alaska crossed by the Fairbanks North profile. At its northwestern termination in east-central Alaska, the Tintina fault is covered by Cenozoic sedimentary rocks but has been interpreted to either: (1) truncate the Beaver Creek and other faults, and in turn be truncated by a northeastward continuation of the Kaltag fault, which is mapped along the southern margin of the Ruby terrane (Grantz, 1966; Grantz and others, 1991); (2) curve southwestward by splaying and joining the Beaver Creek and Victoria Creek faults, which continue southwestward across the Fairbanks North profile (Churkin and others, 1982; Weber, 1990; Dover, 1990); or (3) transform into the northeast-trending thrust faults that are roughly orthogonal to the Fairbanks North profile (Coney and Jones, 1985). The second interpretation is supported by the similarity of the Livengood terrane with the Kandik River terrane in east-central Alaska (Churkin

Geological Society of America Bulletin, v. 106, p. 981–1001, 12 figs., 2 tables, August 1994.

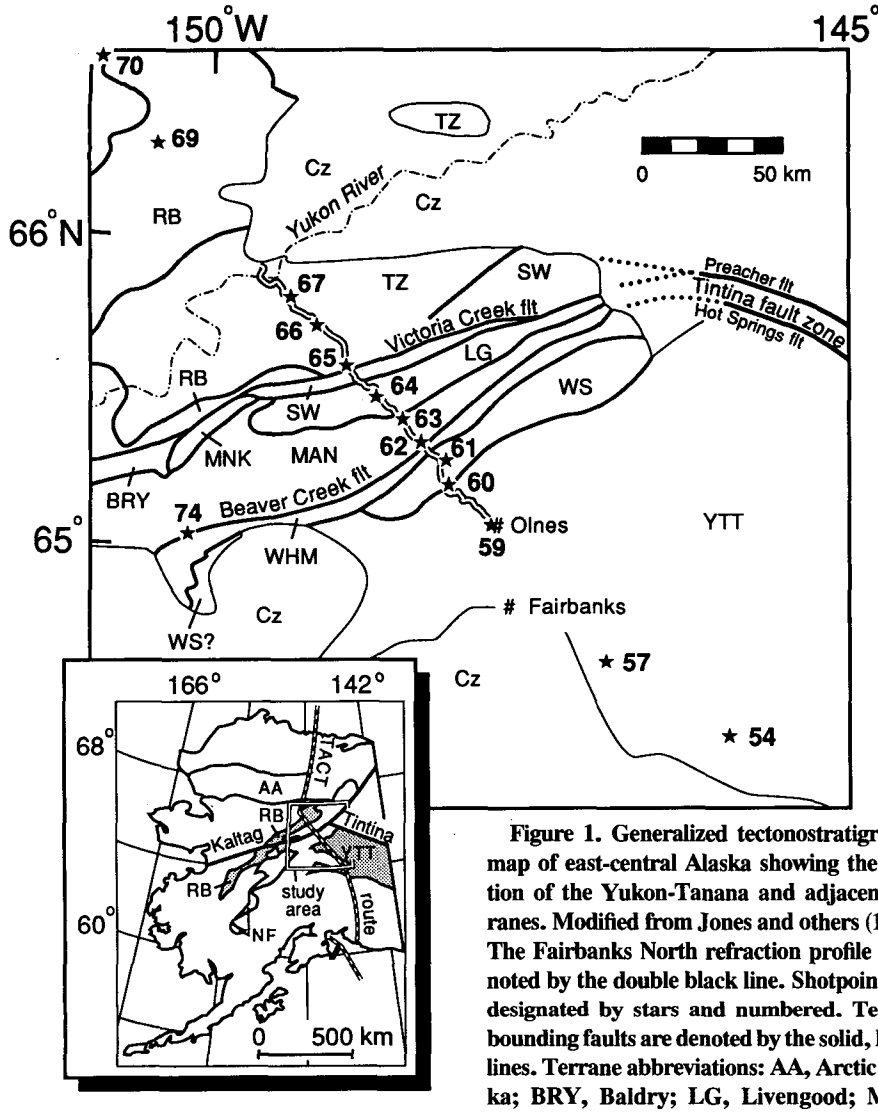

Figure 1. Generalized tectonostratigraphic map of east-central Alaska showing the location of the Yukon-Tanana and adjacent terranes. Modified from Jones and others (1987). The Fairbanks North refraction profile is denoted by the double black line. Shotpoints are designated by stars and numbered. Terrane bounding faults are denoted by the solid, heavy lines. Terrane abbreviations: AA, Arctic Alaska; BRY, Baldry; LG, Livengood; MAN, Manley; MN, Minook; NF, Nixon Fork; RB, Ruby; SW, Mount Schwatka; TZ, Tozitna; WHM, White Mountains; WS, Wickersham; YTT, Yukon-Tanana. Cz indicates Cenozoic sedimentary and volcanic rocks.

and others, 1980) and by the trend of the subparallel Denali fault, which also curves southwestward at about the same longitude.

Although many authors have speculated on the crustal composition beneath this collage of terranes (combinations of one or more of the Yukon-Tanana, Ruby, and Nixon Fork terranes), the only strong evidence for lower crustal composition in this region is based on isotopic and chemical studies. Arth and others (1989) reported isotopic data from Cretaceous plutons intruding the Ruby terrane just north of our profile and concluded that the Ruby terrane in this region is underlain by continental crust.

This paper discusses results of the Fairbanks North profile, a 130-km-long seismic refraction/wide-angle reflection profile that crosses the collage of terranes in the critical region between the Yukon-Tanana and Ruby terranes (Fig. 1). These data, collected in 1987, are part of the U.S. Geological Survey Trans-Alaska Crustal Transect (TACT) project and provide important new information concerning the regional crustal structure, the terranes underlying this area, the nature and locality of the Tintina fault zone, and the inferred tectonic history. First, we give an overview of the geology in the region of our seismic profile, describe the data, and justify the resultant compressional-wave velocity model. Second, this velocity model is discussed in light of existing geologic/tectonic interpretations for the region, and, finally, our interpretation of the velocity model is presented.

GEOLOGIC SETTING

Between the Yukon-Tanana and the Ruby terranes are numerous poorly exposed, small terranes, most of which are elongate in a northeast-southwest direction (Fig. 1). The Fairbanks North profile crosses most of the terranes in this complex region. For describing the geology along the profile, we use terrane nomenclature, modified as noted, from Jones and others (1987) (Table 1). From south to north, the profile crosses the Yukon-Tanana, Wickersham, White Mountains, Manley, Livengood, Mount Schwatka, and Tozitna terranes. In addition to these terranes, the Nixon Fork and Minook terranes lie adjacent to the profile, may occur at depth, and hence are described for completeness.

Yukon-Tanana Terrane

The northern Yukon-Tanana terrane (YTT, Figs. 1 and 2) consists mainly of two highly deformed and regionally metamorphosed sequences (Weber and others, 1978; Foster and others, 1987; Nokleberg and others, 1989): (1) a structurally suprajacent sequence of Late Proterozoic, and older, and early Paleozoic(?) metasedimentary rocks. This sequence consists mainly of regionally metamorphosed and penetratively deformed metasedimentary rocks derived from marl and fine-grained quartz- and clay-rich sedimentary rocks; and (2) a structurally subja-

TABLE 1. TERRANE NOMENCLATURE

Terrane	Jones and others (1987) (terrane)	Churkin and others (1982) (terrane)	Dover (1990) (stratigraphic belt)
Yukon Tanana	Yukon Tanana	Yukon crystalline	N.P.*
Wickersham	Wickersham	Beaver	Wickersham
White Mountains	White Mountains	White Mountains	White Mountains
Manley	Manley	Kandik	Most of the Beaver Creek
Livengood	Livengood	Livengood	Livengood and part of the Beaver Creek
Mount Schwatka	White Mountains and Wickersham	White Mountains and Beaver	Schwatka
Nixon Fork	Nixon Fork	N.P.	N.P.
Tozitna	Tozitna	Tozitna/Circle	Tozitna
Ruby	Ruby	Ruby	N.P.

*Note: not present.

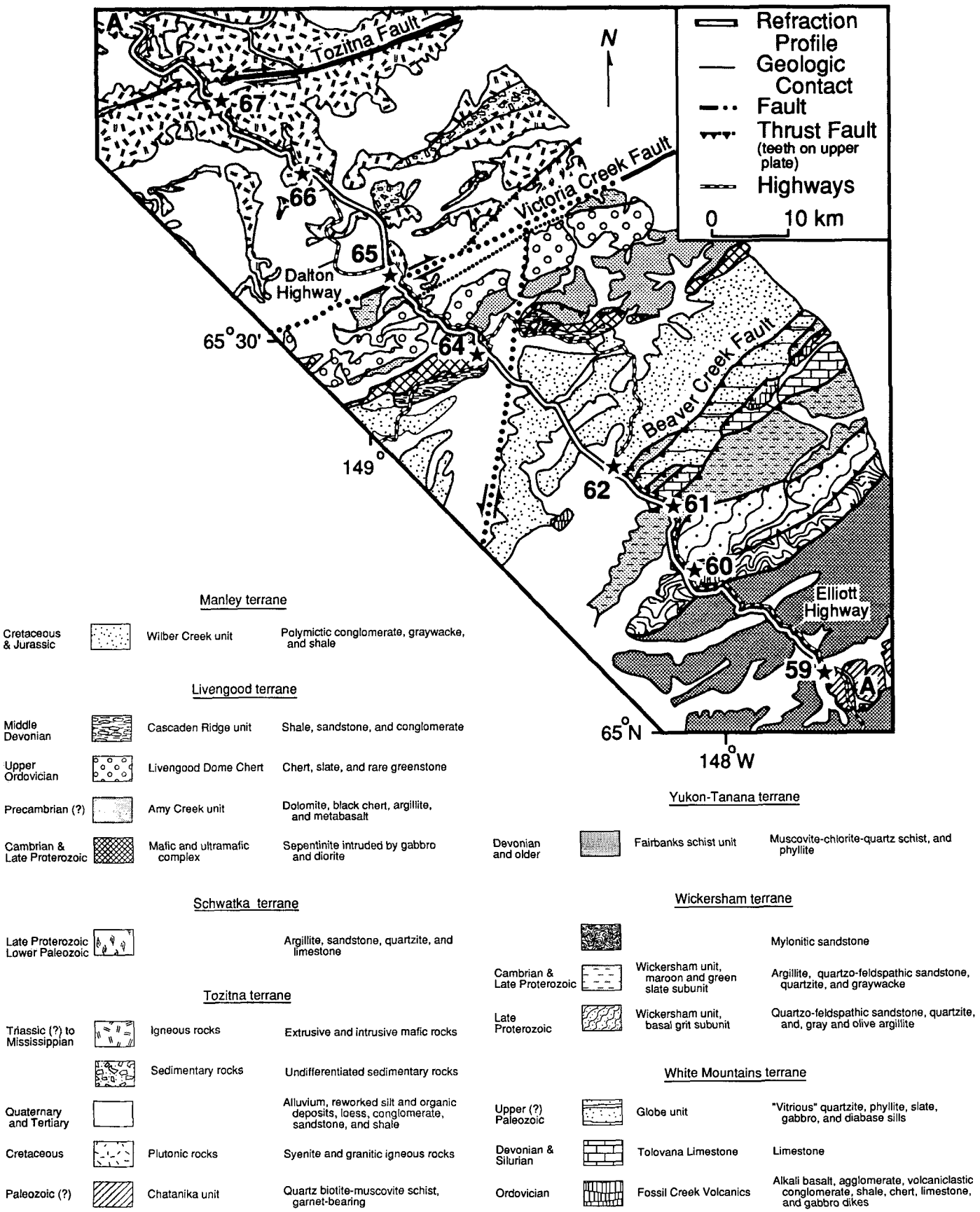

Figure 2. Generalized geologic map and explanation showing the location of the Fairbanks North profile. Adapted from Chapman and others (1971) and Weber (1989).

cent sequence of Devonian and older metasedimentary rocks that contain lenses of metavolcanic and related rocks and locally abundant Devonian metagranitic rocks. Sparse granitic plutons of Late Cretaceous and/or early Tertiary age intrude the northern Yukon-Tanana terrane.

Wickersham Terrane

The Wickersham terrane (WS, Figs. 1 and 2) is interpreted as a marine, continental margin sequence that consists of Late Proterozoic and Lower Cambrian interbedded granule and pebble conglomerate, argillite, and quartzo-feldspathic sandstone that contain sedimentary structures characteristic of turbidites (Churkin and others, 1982; Weber and others, 1985; Jones and others, 1987; Moore and Nokleberg, 1988; Dover, 1990). Wickersham rocks may be depositional basement for the White Mountains and Livengood terranes to the northwest (Dover, 1990) or may be a fault sliver unrelated to these terranes (Churkin and others, 1982; Jones and others, 1986). The Wickersham terrane overlies the Yukon-Tanana terrane on a north-dipping contact. This contact between the Wickersham terrane and the Yukon-Tanana terrane is controversial and may be either an important structural break or a gradational contact (Churkin and others, 1982; Grantz and others, 1991). The Wickersham terrane is juxtaposed against the White Mountains terrane along a contact of uncertain nature, but likely a fault.

White Mountains Terrane

The White Mountains terrane (WHM, Figs. 1 and 2) consists of the Fossil Creek Volcanics and the Tolovana Limestone (Dover, 1990). Although interpreted as a volcanic arc by Churkin and others (1982), the Fossil Creek Volcanics are more likely a sequence of Ordovician silicic sediments rich in alkali basaltic submarine flows and volcaniclastic rocks that were deposited either on a continental margin or an oceanic seamount (Jones and others, 1987; Wheeler and others, 1987; Dover, 1990). These rocks may have been deposited on a basement of upper Wickersham terrane. The Fossil Creek Volcanics are overlain by the Tolovana Limestone on a contact that has been interpreted either as gradational (Churkin and others, 1982; Blodgett and others, 1987) or unconformable (Dover, 1990). The Tolovana Limestone consists of Silurian and Devonian dolomite and limestone that is interpreted as a carbonate bank deposit (Churkin and others, 1982; Jones and others, 1987). The Tolovana Limestone is thrust over the Globe unit, which consists of sheared recrystallized(?) quartzose sandstone and argillite intruded by abundant sills of diorite and gabbro (Weber and others, 1985; Dover, 1990) of Triassic age (J. Mortensen, 1991, personal commun.).

Manley Terrane

The Manley terrane (MAN, Figs. 1 and 2) is interpreted as a turbidite flysch basin (Churkin and others, 1982) consisting mainly of flyschoid rocks and chert-rich conglomerates (Dover, 1990). Two units compose the Manley terrane: (1) the Vrain unit (Foster and others, 1983), a Triassic(?) or Jurassic(?) (F. Weber, 1991, oral commun.) unit of carbonaceous, fine-grained to gritty clastic rocks, and (2) the Wilber Creek unit (Weber and others, 1985), a Late Jurassic to Early Cretaceous unit of shale, graywacke, quartzite, and conglomerate. Late Cretaceous and Tertiary granitic rocks and gabbros of unknown age intrude the Manley terrane (Jones and others, 1987). The Manley terrane is juxtaposed against the White Mountains terrane to the south along the Beaver Creek fault, which is interpreted as a south-dipping thrust fault (Churkin and others, 1982; Weber, 1989; Dover, 1990). Although the contact is not exposed, map relationships suggest that the Manley terrane lies depositionally on the Livengood terrane to the north.

Livengood Terrane

The Livengood terrane (LG, Figs. 1 and 2) (Churkin and others, 1982) consists of four units: (1) a mafic and ultramafic complex of gabbro, diabase, and sepentinite that yield Cambrian K-Ar ages (Loney and Himmelberg, 1988); (2) the Livengood Dome Chert of Late Ordovician age, composed of chert and siliceous argillite that locally contains graptolites (Chapman and others, 1980); (3) the Amy Creek unit of unknown age that consists of dolomite, chert, shale, and sparse mafic volcanic rocks (Weber and others, 1985); and (4) the Middle Devonian Cascaden Ridge unit composed of siltstone, shale, sandstone, and conglomerate turbidites (Weber, 1989). The Livengood terrane is interpreted as either a continental margin deposit (Churkin and others, 1982) or a less volcanic-rich equivalent of the White Mountains terrane (Dover, 1990).

Minook Terrane

The Minook terrane (MNK, Fig. 1), which has lithology similar to the Beaver Creek stratigraphic belt of Dover (1990) (that is, the Manley terrane), consists of upper Paleozoic flysch and minor chert-pebble conglomerate (Jones and others, 1987).

Mount Schwatka Terrane

The Mount Schwatka terrane (SW, Figs. 1 and 2) is equivalent to the combined portions of the White Mountains and Wickersham terranes of Jones and others (1987) north of the Victoria Creek fault, and to the Schwatka stratigraphic belt of Dover (1990). The Mount Schwatka terrane consists of argillite and quartz-rich sandstone, granule and pebble conglomerate, and black limestone of Late Proterozoic and/or early Paleozoic age that are unconformably(?) overlain by interlayered Devonian limestone and mafic volcanic rocks (R. B. Blodgett, 1992, oral commun.).

Nixon Fork Terrane

The large Nixon Fork terrane (NF, Fig. 1) lies southwest of the Fairbanks North profile on strike with the Manley and Livengood terranes. The Nixon Fork terrane consists of a late Precambrian basement of mainly pelitic and calcareous schists that are intruded by Early Proterozoic metagranitic rocks and capped by Late Proterozoic felsic metavolcanic rocks. The overlying sedimentary cover rocks consist of Cambrian limestone and clastic rocks, Ordovician and Devonian carbonate platform rocks, and Permian, Triassic, and Cretaceous clastic sedimentary rocks. On the basis of its inferred northeast plunge, Grantz and others (1991) proposed that the Nixon Fork terrane is present at depth under the Fairbanks North profile and may be equivalent to the Minook terrane.

Tozitna Terrane

The Tozitna terrane (TZ, Figs. 1 and 2) was interpreted as a dismembered ophiolite (Churkin and others, 1982), although the lower ultramafic-to-gabbroic part of a typical ophiolitic sequence has not been identified. More recent work interprets the terrane as a tectonic assemblage of upper-crustal oceanic rocks, particularly seamounts (Patton and Box, 1989; Grantz and others, 1991). The Tozitna terrane consists primarily of mafic volcanic rocks, pillow basalts, diabase, and gabbro assigned to the Rampart Group (Brosgé and others, 1969). Interbedded with or intruded by the mafic rocks are subordinate chert, argillite, tuffaceous and volcaniclastic rocks, siltstone, sandstone, and minor limestone of Mississippian, Permian, and

Triassic age. The mafic rocks are alkalic to subalkalic in composition; rare cumulate ultramafic layers and lenses are observed (Cady, 1987).

Ruby Terrane

The Ruby terrane (RB, Figs. 1 and 2) is lithologically similar to the Yukon-Tanana terrane. It consists of Paleozoic and older metasedimentary and Devonian metaigneous rocks intruded by abundant mid-Cretaceous plutons (Nokleberg and others, 1989; Patton and others, 1989; Dover, 1990). The Ruby terrane is overthrust by the Tozitna terrane (Patton and others, 1989; Dover, 1990).

Faults Between Terranes

Most terrane-bounding contacts in this region are unexposed but are interpreted as shallowly to moderately southeast-dipping Mesozoic thrust faults (Dover, 1990). Steeply dipping faults, including the Victoria Creek and Tozitna faults (Fig. 2), offset some terranes and are interpreted by some workers to be westward extensions or splays of the northeast-trending Tintina fault system (Dover, 1990; Weber, 1990). In addition, Weber (1989, personal commun.; 1990) postulated that, to the east, a more southerly strand of the Tintina fault system, the Hot Springs strand, curves to the southwest and crosses the Fairbanks North profile near the southeast boundary of the Manley terrane, where it has been buried by younger thrust plates of the White Mountains terrane.

PROFILE DESIGN

The Fairbanks North profile extends from Olnes to the Yukon River along the Elliott and Dalton highways and portions of the Trans-Alaska oil pipeline right-of-way (Fig. 2). Approximately one-fifth of this 130-km-long profile is in the Yukon-Tanana terrane, whereas the remaining four-fifths crosses the Wickersham, White Mountains, Manley, Livengood, Mount Schwatka, and Tozitna terranes to the northwest (Figs. 1 and 2). A total of nine in-line and four off-end shots, and one fan shot (shotpoint 74), with offsets ranging from 0 to 240 km, were recorded by instruments spaced at 1-km intervals. This configuration provides reversed coverage of all primary crustal and upper mantle phases. The sound sources consisted of explosive charges ranging from 227 to 2,724 kg detonated in 50-m-deep drill holes or shallow (3–15 m) lakes. For additional information on experimental design and initial processing, see Beaudoin and others (1989, 1992).

Of the nine in-line shots, six produced sufficient energy to be recorded at all instrument sites. Shotpoints 61 and 66 had poor coupling and were only recorded to distances of ~10 km. Although the data from these two shots were used to define the surface velocity structure, they are not discussed or presented here. Additionally, shotpoint 63 detonated improperly and was not recorded by the array.

COMPRESSIONAL-WAVE VELOCITY MODEL

Results from the Fairbanks North profile reveal a crustal velocity structure that can be subdivided into three upper-crustal and at least two lower-crustal domains. The three upper-crustal domains are separated by prominent, lateral, low-velocity anomalies (centered at model coordinates 145 and 195 km) (Fig. 3). The northern and southern domains have similar velocity structures, including regions of strong, lateral and vertical velocity gradients and overall higher velocities than the central domain. The central domain has no apparent strong velocity gradients within it. A midcrustal reflector underlies the central and northern upper-crustal domains. A correlation between the upper-crustal low-velocity zones and the topography and reflection character of this midcrustal reflector suggests that these structures continue at least to mid-crustal depths. The Moho reflection is prominent beneath the profile and shows a division in character between the north and south. The southern portion of the Moho has a reflection character indicative of a thick transition zone as opposed to the northern section that has a reflection character more in keeping with a sharp velocity-discontinuity. This difference of the Moho reflection character between north and south is interpreted as evidence that at least one of the prominent upper-crustal faults cuts the entire crust. Below, we present the data, modeling, and discussion that support these interpretations.

TRAVELTIME MODELING

Modeling Approach

To model these data, a coupled inverse/forward modeling approach was chosen (see Beaudoin, 1992). For the upper 12 km of crust (layer 1), where velocity is well controlled and phase arrivals are clear, we used a nonlinear, least squares inverse method (Nowack and Lutter, 1988; Lutter and others, 1990) to fit only the refracted arrivals from shots 59 through 67. For the middle and lower crust, where velocity is less well constrained, where the arrivals are often difficult to correlate, and where user interaction and discrimination are important, we used iterative ray trace forward modeling (Červený and others, 1977; Luetgert, 1988, 1992) to fit both refracted and reflected arrivals from all shots. The upper crustal inverse model was the starting model for the middle and lower crustal forward modeling between shotpoints 59 and 67. For off-end shotpoints 54 and 57, the velocity model from Beaudoin and others (1992) was used (Fig. 3B). For the northern off-end shotpoints, shotpoints 69 and 70, we extrapolated the velocity function beneath shotpoint 67 to these locations.

The final product of this combined technique is a model with a well-resolved, 8 km upper-crustal section (Fig. 3A) and an average traveltime fit ≤50 ms. For the middle to lower crust and upper mantle, errors in traveltime fit of 0.1–0.2 s are considered significant. Hence, by perturbing the forward model for the middle and lower crust to cause traveltime misfits as large as 0.1–0.2 s, we determined the uncertainties in the middle and lower crustal model parameters (Table 2).

Phase correlations present the most ambiguous step in refraction data interpretation (Mooney and Prodehl, 1984). Phases were correlated by first picking the direct/refracted arrivals and noting significant changes in slope along these traveltime branches. Where changes of slope occurred, the data were examined for reflected phases associated with these changes in velocity. The strongest reflections are picked first and used as templates for identifying these reflections on reversing shots. In order to build an internally consistent model, only those reflections convincingly identified along the profile were retained for the modeling. Reflections that could not be tracked along the profile are considered to be local.

Upper Crust

The first prominent velocity change in the refracted arrival is in the shot-to-receiver offset range of 5–20 km (Figs. 4–7 and Appendix). Although this indicates a change in velocity structure, no clear reflection is associated with this change in slope. Therefore, we elected to combine all refractions (Pg) from shot-to-receiver offsets of 0 to 40–70 km (see below) into a single "layer,"

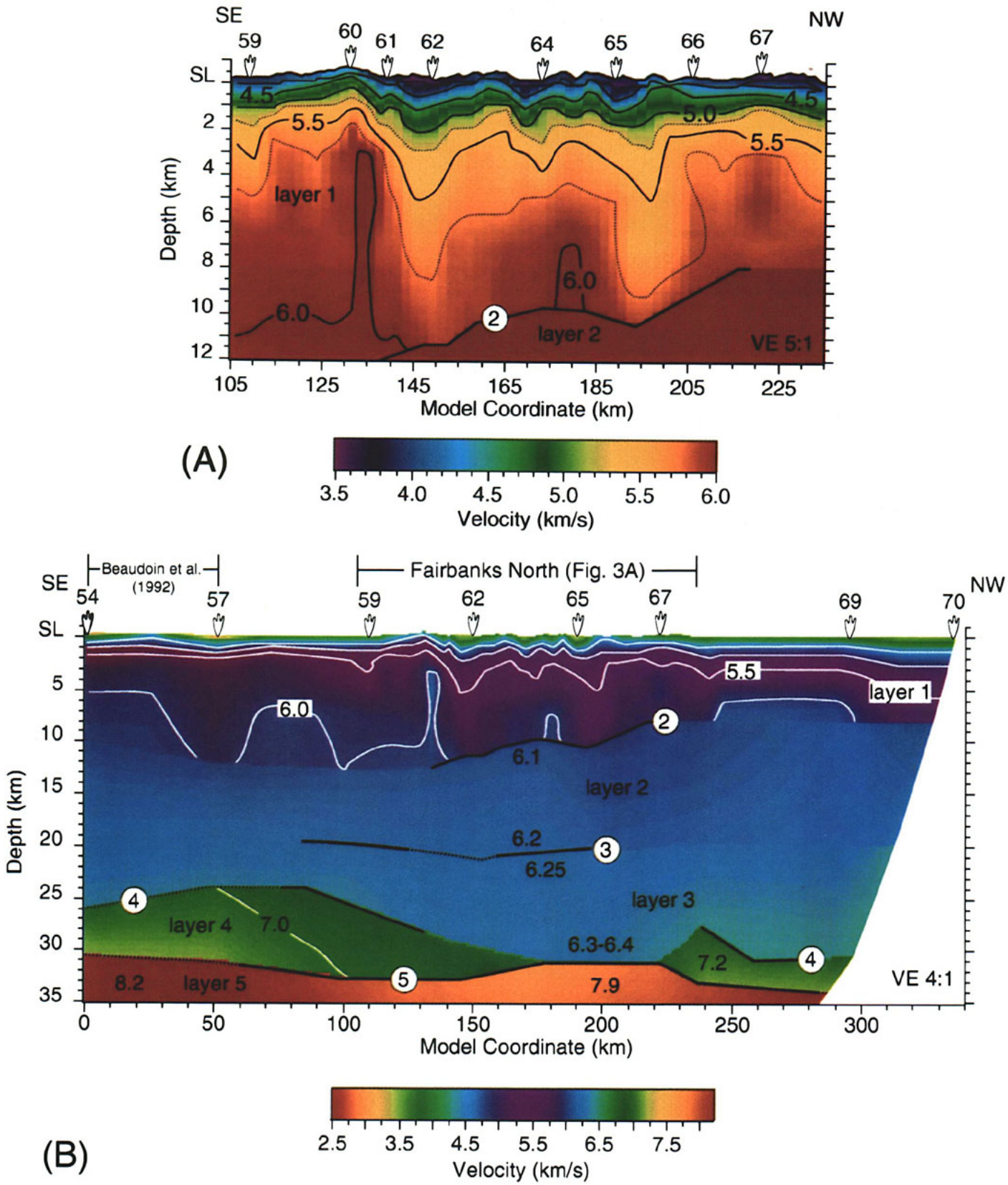

Figure 3. Compressional-wave velocity model for crust beneath the Fairbanks North profile. (A) Contoured model (inverse model) of the upper 12 km of crust. (B) Contoured model for the crust (coupled inverse and forward model, see text). Contours are the solid and dotted curved lines. Interfaces are straight line segments, solid where controlled by reflections and dotted where inferred or controlled by the model of Beaudoin and others (1992). Regions of color represent ray coverage from both this study and Beaudoin and others (1992).

TABLE 2. MODEL UNCERTAINTIES

Interface and layer	Interface depth uncertainty (km)	Layer velocity uncertainty (km/s)
2	±0.5	±0.1
3	±1.0	±0.2
4	±1.5	±0.2
5	±2.5	±0.2

layer 1. Pg is variable in amplitude along the profile, reflecting both changes in the subsurface velocity field and the near-surface geology. Pg also has trace-to-trace time shifts of up to 200 ms due to velocity variations in the near surface. Two lateral velocity anomalies, which divide the upper crust into three domains, are indicated by asymmetric traveltime branches of Pg for shotpoints 62 and 65 (Fig. 5).

Middle and Lower Crust

Demarcating the onset of mid-crustal arrivals are a clear reflection (PcP; interface 2) on shotpoints 65 and 67 (Figs. 6A and 7A), a

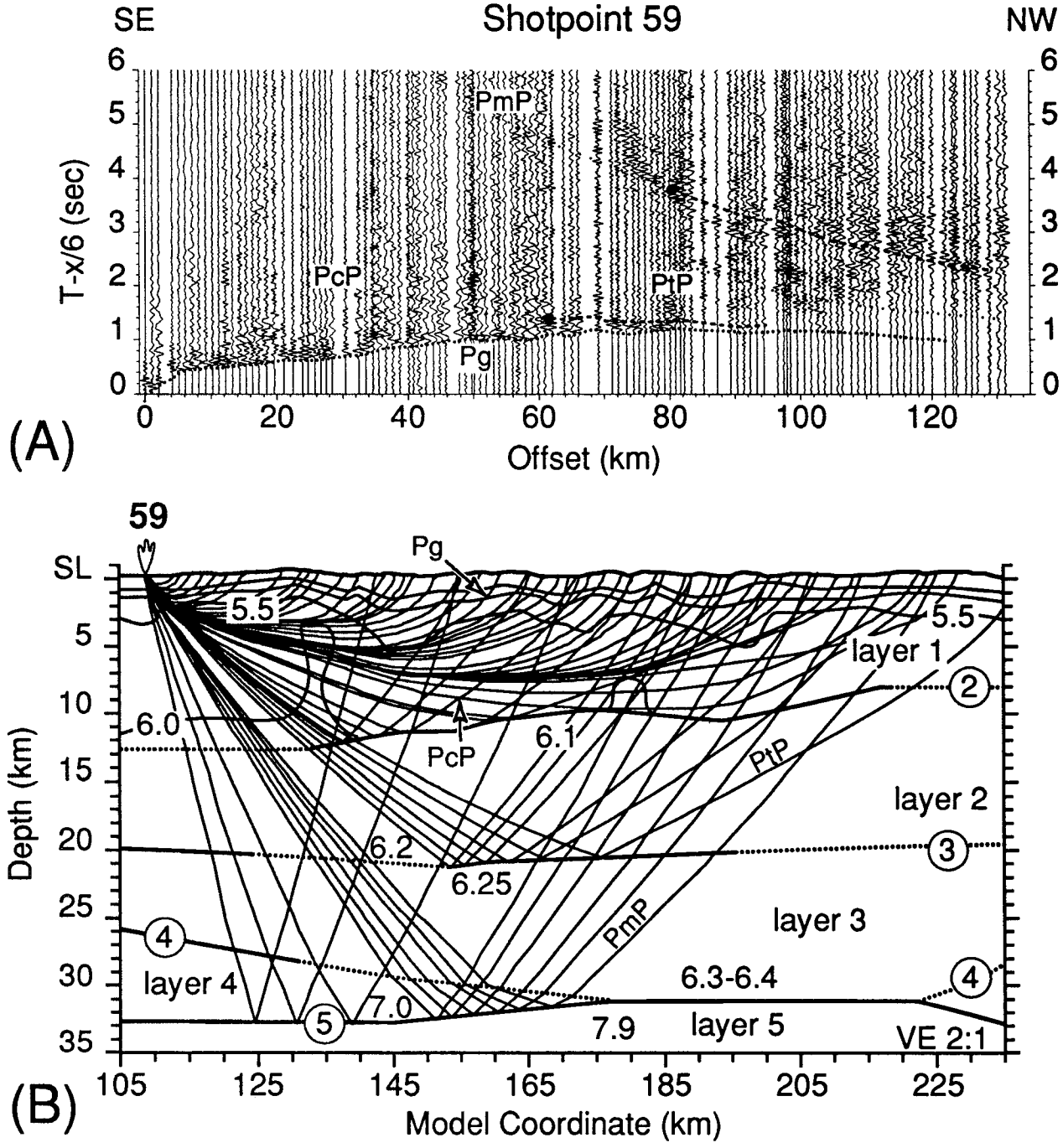

Figure 4. Record section and ray diagrams for shotpoint 59. (A) Trace-normalized record section with the calculated traveltimes from the final velocity model. Refractions are represented by the closely spaced dotted lines, precritical reflections by the widely spaced dotted lines, and postcritical reflections by the dashed lines. Critical points, theoretical locations for the first existence of an associated refracted arrival, are denoted by the solid circles. (B) Ray diagram for the traveltimes presented in part A.

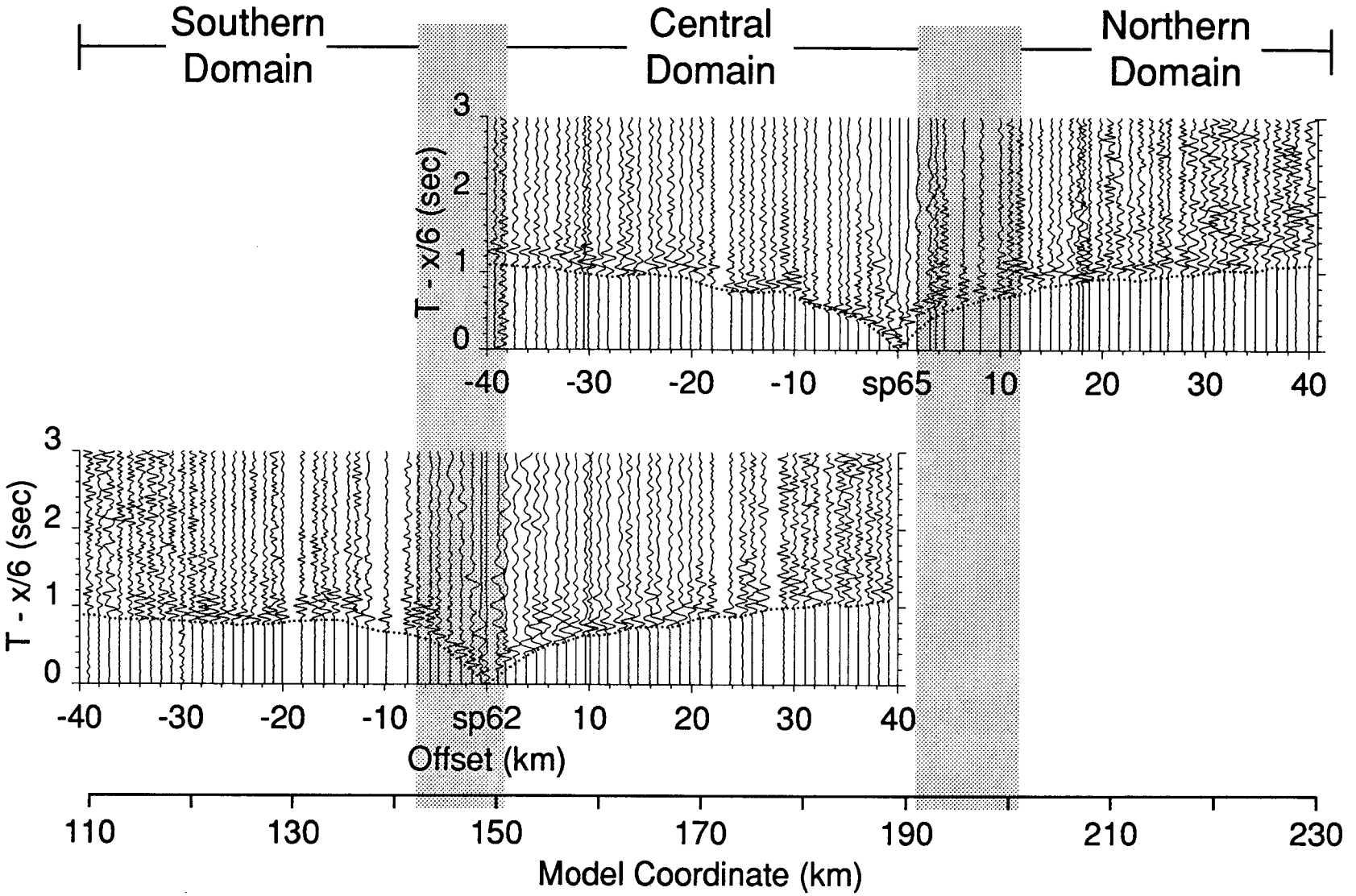

Figure 5. Record sections showing the asymmetry of the first arrivals (Pg) for shotpoints 62 and 65. The data are plotted in trace-normalized format with the calculated traveltimes for Pg from the final velocity model overlain. The gray bands denote the locations of the strong lateral low-velocity anomalies in the model.

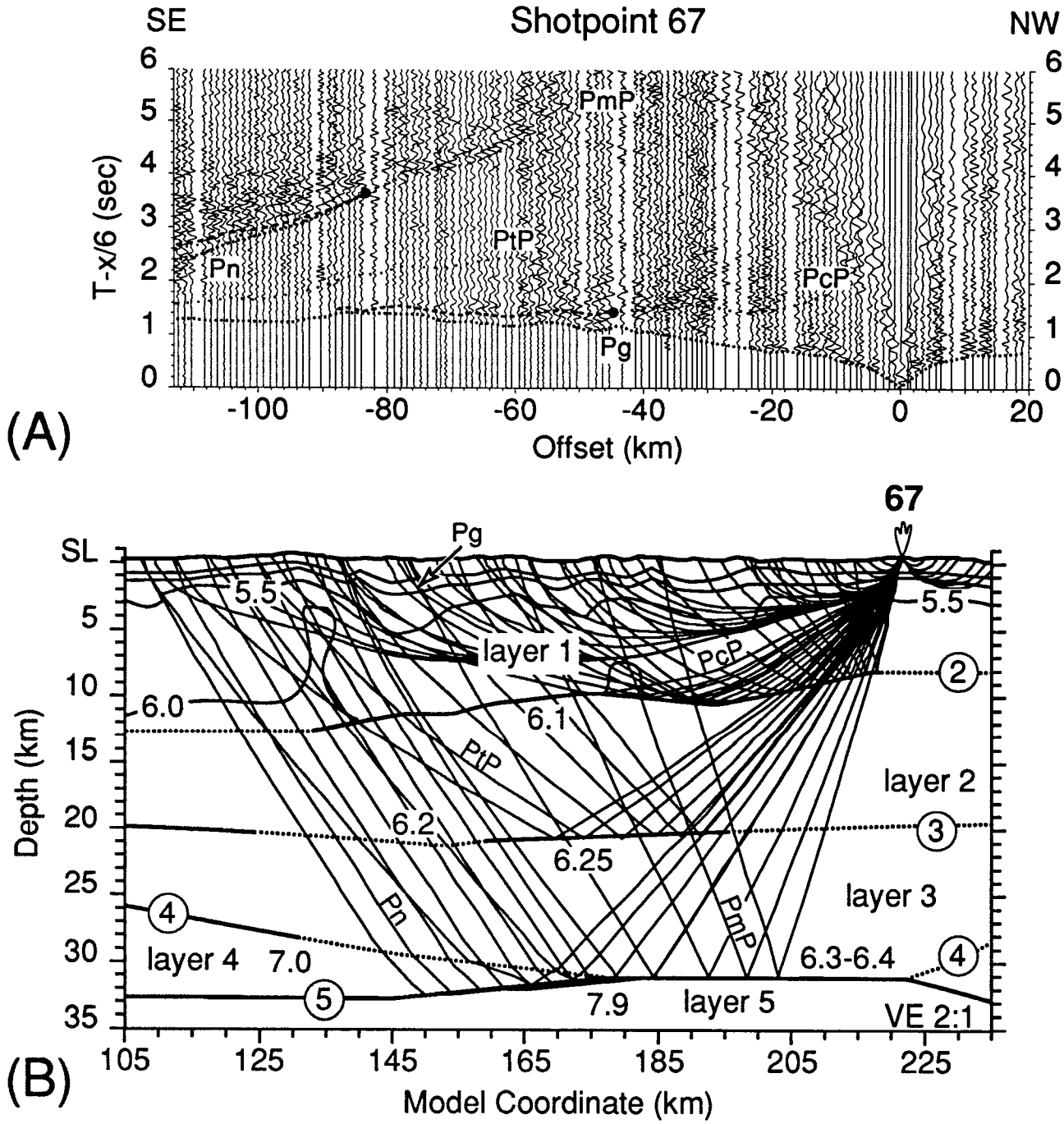

Figure 6. Record section and ray diagrams for shotpoint 67. (A) Trace normalized record sections. See caption to Figure 4 for explanation. (B) Ray diagram for the traveltimes presented in Figure 6A.

weak reflection on shotpoints 59, 62, and 64, and a poorly defined reflection on shotpoint 60 (Fig. 4A and Appendix). Based on the offset location of the PcP reflection, a refracted arrival from interface 2 should become the first arrival at a distance of 40–50 km on the northern end of the profile and at 60–70 km on the southern end of the profile. Subsequent modeling, however, indicates that the geometry of the PcP reflector and the velocity variation above and below interface 2 are such that Pg and the refracted phase from interface 2 are indistinguishable in traveltime. The variation in offset location of the PcP reflection from south to north does indicate a shallowing of the PcP reflector northward (Fig. 3A).

The geometry of the PcP reflector, interface 2, is well constrained on the northern end of the profile and less well constrained on the southern end of the profile. Along the northern end of the profile, PcP is well defined both pre- and postcritically on shotpoints 65 and 67 (Figs. 6 and 7). Along the southern end of the profile, at shotpoints 59–64, PcP is difficult to correlate and is identified only for short distances (Fig. 4A and Appendix). Therefore, from model coordinates 135 to 185 km, this interface is less well defined in depth, and the velocity structure for

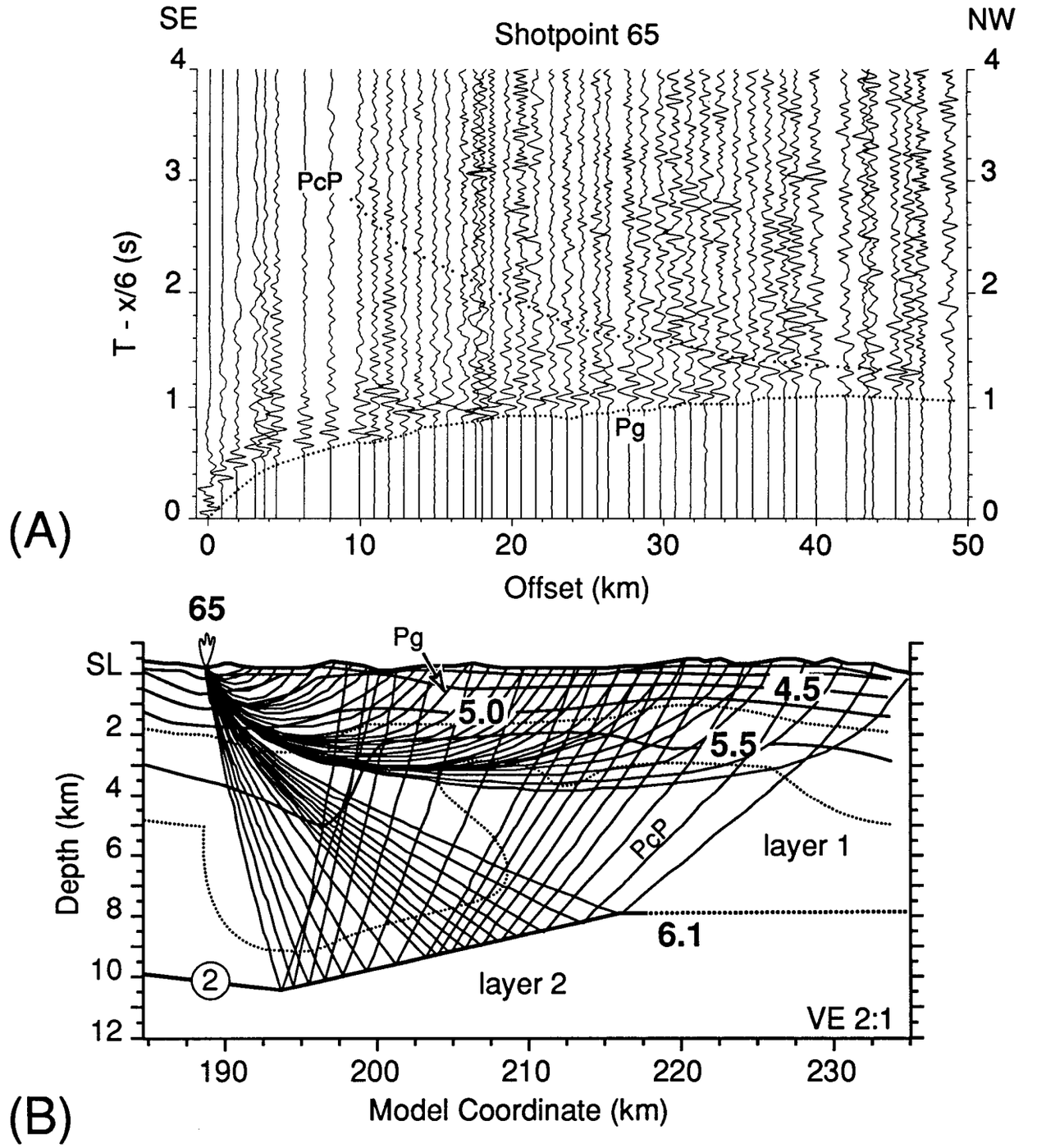

Figure 7. Record section and ray diagram for shotpoint 65. (A) Trace normalized record section. See caption to Figure 4 for explanation. (B) Ray diagram for the traveltimes presented in Figure 7A.

the interval directly above it is not well controlled. In contrast, between model coordinates 185 and 220 km, the interface depth and shape and the velocity directly above it are well constrained. The 6.5° ± 2.5° southward apparent dip northwest of shotpoint 65 is required to fit the variable traveltimes for this phase between shotpoints 65 and 67 (Figs. 6 and 7). Based on our forward modeling, velocities for layer 2 range from 6.0–6.1 km/s at its top to 6.2–6.25 km/s at its base. Although these velocities are not well constrained, velocities at the top of this layer cannot exceed 6.3 km/s without producing a prominent, calculated first arrival well ahead of the observed first arrival.

The next phase interpreted is PtP, a weak reflection from the lower crust. This reflection is best seen on shotpoint 67 (Fig. 6A), where it is associated with an increase in reflection amplitudes in the offset range of 70–110 km between ~1.5 and 2.5 s. The reversing shot, shotpoint 59, exhibits a less-well-defined PtP reflection (Fig. 4A). In ad-

dition to these two shots, this phase is identified on in-line shots 60 and 65 (Appendix) and off-end shot 57 (Fig. 8A). The strength and coherence of this phase is variable across the profile, and no systematic pattern is evident.

The PtP reflector, interface 3, is best constrained in depth by shotpoints 57 (Fig. 8) and 67 (Fig. 6). A reflection from this interface is not apparent from shotpoint 69, and therefore interface 3 is modeled to have a northern termination at approximately model coordinate 195 km. We have terminated the southern extent of this interface at about model coordinate 80 km (beneath shotpoints 54 and 57; Beaudoin and others [1992] do not model an interface at this depth). From model coordinates 125 to 155 km, this interface has no observed reflection. Velocities within layer 3 are based on the wide-angle reflection from interface 4, PiP, that should asymptotically approach the maximum velocity of layer 3 at the farthest offsets. These velocities are modeled as 6.25 km/s at the top to 6.3–6.4 km/s at the base; velocities ≥6.6 km/s at the base of this layer produce discernible traveltime misfits for the PiP reflection.

The next interpretable phases, Pi and PiP, are refractions and reflections, respectively, from the lower crust and are largely constrained by the off-end shots. Beaudoin and others (1992) modeled a basal crustal layer beneath shotpoints 54 and 57 based on a refraction/wide-angle reflection profile collected between Fairbanks and Delta Junction. A similar basal crustal reflection (PiP) is identified on shots 57 and 69 (Fig. 8 and Appendix). Although these two shots originate in different geologic settings, an overall match in the first-break traveltime curves and postcritical PiP (shotpoint 57) and PmP (shotpoint 69) traveltime curves indicates similar average crustal velocities. Pi is identifiable only on shotpoint 57 (Fig. 8B). Shotpoint 69 should have recorded Pi, but either the signal-to-noise ratio is too small, or Pi is not present. In-line shotpoints 59, 60, and 67 have sufficient offsets to record the PiP reflection. There is no evidence, however, of PiP on shotpoints 60 and 67, and strong but discontinuous energy on shotpoint 59 does not lend itself to modeling.

The absence of the PiP reflection on the in-line shot profiles suggests either that the PiP reflector (interface 4) is not continuous beneath the profile (the layer pinches out) or that a poor signal-to-noise ratio prevents us from identifying this reflection. Although the data are not sufficient to determine the continuity of layer 4 definitively, we chose to model the layer pinching out. This decision is influenced by the systematic change in PmP character across the profile. In the region of our model where layer 4 is nonexistent, PmP is a strong, largely unicyclic phase; where layer 4 exists, PmP is poorly defined and difficult to correlate (Fig. 9). In addition to this observation, Pi and PiP traveltimes from shotpoint 57 require that layer 4 extend beneath the instrument array to approximately model coordinate 175 km. From the north, shotpoint 69 has two distinct lower-crustal arrivals, identified as PiP and PmP. PiP shows an abrupt truncation at an offset of 100 km from the shotpoint (Appendix). We attempted to model this with one-dimensional synthetic seismograms by lower-crustal destructive interference of the wavefield at far offsets. We could not, however, match the observed amplitudes for this shot. Based on these tests, we favor a model where layer 4 pinches. Velocities within this layer are 6.9–7.2 km/s and are constrained by modeling PmP traveltimes from shotpoint 57 (Fig. 8). This result also agrees with the velocities determined by Beaudoin and others (1992).

The Moho reflection (PmP) is well represented at distances ≥60 km from all shotpoints and also shows a variable character from the in-line shotpoints, exhibiting a systematic change from north to south (Fig. 9). Receivers recording PmP reflections bottoming north of approximately model coordinate 175 km are strong, coherent, and often multicyclic. PmP reflections bottoming south of model coordinate 175 km are discontinuous and less coherent. Although some ambiguities arise in modeling the geometry of the Moho (interface 5) due to the discontinuous nature of the PmP reflection along the southern end of the profile, continuous segments (5–10 km in length) exist where the traveltimes are so well defined as to give confidence that we have modeled the Moho correctly. The modeled Moho depth averages 32 km beneath the profile. Minor topography on this interface is within modeling errors. We model, however, a shallowing of the Moho to 31 km depth along model coordinates 175–220 km and a deepening of the Moho to as much as 34 km north of shotpoint 67.

The upper-mantle refraction (Pn) is weak and emergent on shotpoints 54 and 57 (Appendix and Fig. 8B) and not easily identified on shotpoints 69 and 70 (Appendix). Beaudoin and others (1992) describe a similar Pn character from mantle beneath shotpoints 54 and 57 and attribute it to a weak velocity gradient in the uppermost mantle; we believe a similar interpretation explains the Pn character for shotpoints 54 and 57. This difference in Pn from south to north may, in part, be due to poor shot coupling; both shotpoints 69 and 70 have a lower signal-to-noise ratio than shotpoints 54 and 57.

The upper-mantle velocity structure is best defined by the southern off-end shotpoints, shotpoints 54 and 57 (Appendix and Fig. 8) and earlier work (Beaudoin and others, 1992). The Pn velocity beneath shotpoints 54 and 57 is 8.2 km/s based on this earlier work. By holding this velocity fixed, the data require a decrease in Pn velocity to 7.9 km/s under the profile to satisfy the observed traveltimes for shotpoints 54 and 57; this result is in accordance with Pn traveltimes from shotpoints 69 and 70 (Appendix), albeit poorly controlled due to poor signal-to-noise ratios for these shotpoints. Significant traveltime errors occur if a constant 8.2 km/s is used for the upper mantle velocity beneath the profile.

DISCUSSION AND INTERPRETATION

Velocity Structure Implications

The two strong, lateral low-velocity anomalies centered at 145 km (southern) and 195 km (northern) divide the upper crust into three domains (Figs. 3A and 10). The southern and northern domains have higher velocities and stronger velocity gradients than the central domain. Beneath this tripartite upper crust, the middle to lower crust exhibits at least two domains based on the character of the Moho reflection and the presence or absence of a basal crustal layer (layer 4). Below, we discuss these upper- and lower-crustal domains in light of the geology of the region between the Yukon-Tanana and Ruby terranes.

Upper-Crustal Faults and Terranes. The upper-crustal, lateral, low-velocity anomalies contain or are adjacent to the Beaver Creek and Victoria Creek faults, faults that may represent strands of the Tintina strike-slip fault (Fig. 10). The southern velocity anomaly defines a vertical (90° ± 10°) structure, based on velocity minima, that projects to the surface at the Beaver Creek fault, suggesting that the Beaver Creek fault may be near-vertical. Alternatively, the Beaver Creek fault may be a thrust fault that has buried an older continuation of the Hot Springs fault (F. R. Weber, 1989, written commun.; Weber, 1990; Weber and others, 1992). The northern anomaly is defined by two lobes: a main lobe centered at model coordinate 195 km at 2–10 km depth, and a near-surface lobe centered at model coordinate 187 km at ≤2 km depth (Figs. 3A and 10). The shallow lobe corresponds to the mapped trace of the Victoria Creek fault and is offset by 8–10 km southeast of the main lobe. Two interpretations of crustal structure

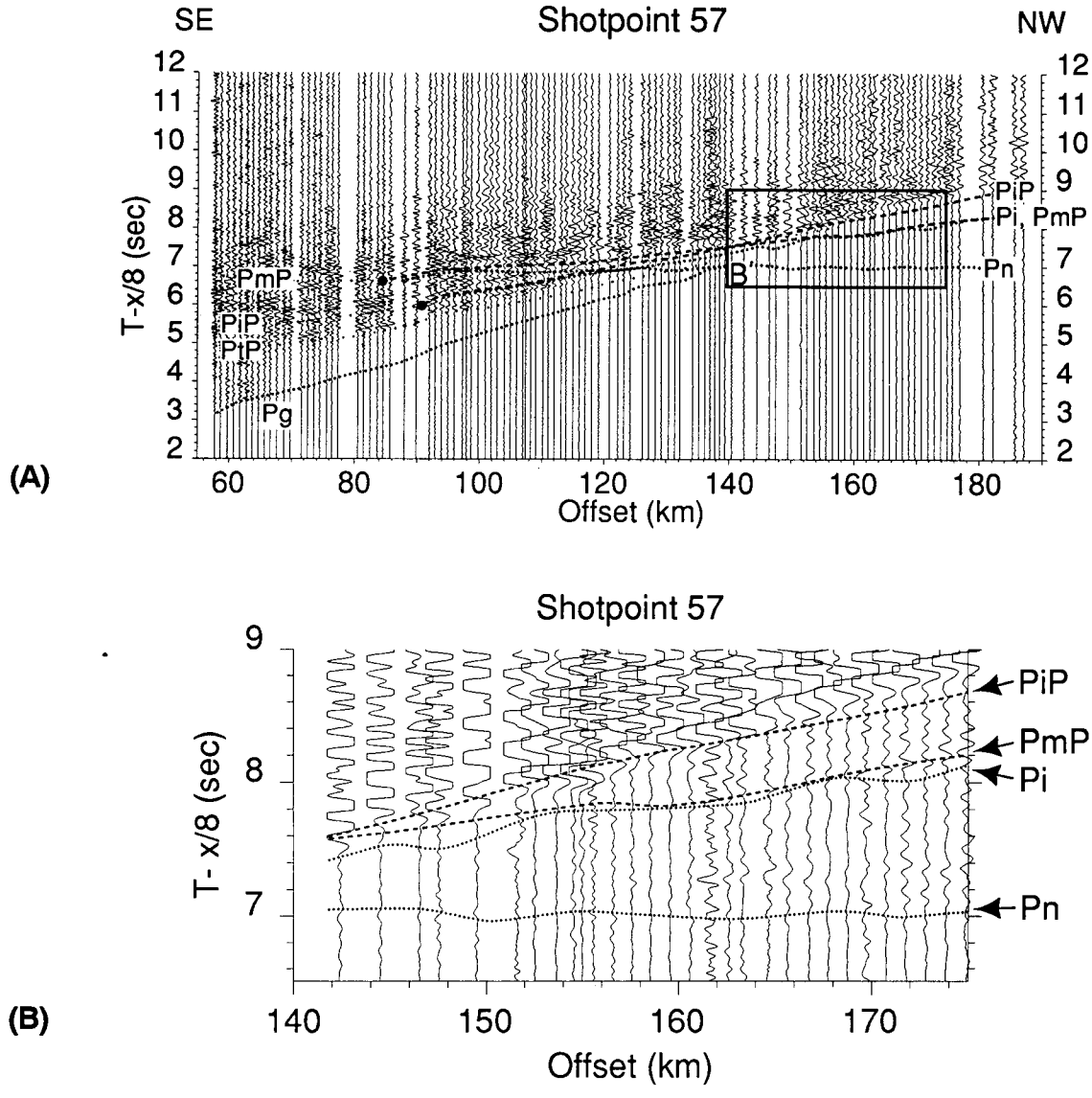

Figure 8. Record section and ray diagrams for shotpoint 57. Box shows area in following frame. (A) Trace normalized record section. See caption to Figure 4 for explanation. (B) A blow-up showing Pi and Pn for shotpoint 57. (C) Ray diagrams for the traveltimes presented in Figures 8A and 8B.

are possible and dependent on how these lobes are related: (1) If the shallow and main lobes define the same feature, the data suggest that the Victoria Creek fault has an apparent northwestward dip of ~45° beneath our profile. (2) If the shallow and main lobes do not define the same feature, the Victoria Creek fault is the near-vertical southern boundary of an upper-crustal, low-velocity body (main lobe). We favor the first interpretation, a northward dipping Victoria Creek fault, because foliation in schistose rocks along the north side of the Victoria Creek fault northeast of our study area dip steeply to the north (Weber and others, 1992; T. E. Moore, unpub. data) and because Jones and others (1986), who conducted structural studies along the Victoria Creek fault west of our profile, concluded the fault dips northward. An alternate explanation for the main lobe of low velocity, the second interpretation, is suggested by a corresponding discontinuity in the aeromagnetic data that separates mainly sedimentary, nonmagnetic units of the Rampart group to the south from mainly igneous, magnetic units of the Rampart group to the north (Cady, 1991). This would require that the main lobe be a steeply dipping body of low-velocity sedimentary rocks. The thickness of the main lobe (8 km), however, is contrary to the thickness of these sedimentary rocks, which are thought to be relatively thin (for example, Weber, 1992).

The southernmost domain's principal upper-crustal feature is a region of high velocity at model coordinate 130–135 km. This region underlies the Wickersham and White Mountains terranes, which are characterized by southeast-dipping strata that have been mylonitized along a northwest-dipping contact between the Wickersham and Yukon-Tanana terranes. The velocity high is consistent with the presence of higher-grade rocks to the southeast in the Yukon-Tanana terrane and northwest-dipping mylonitic metamorphic

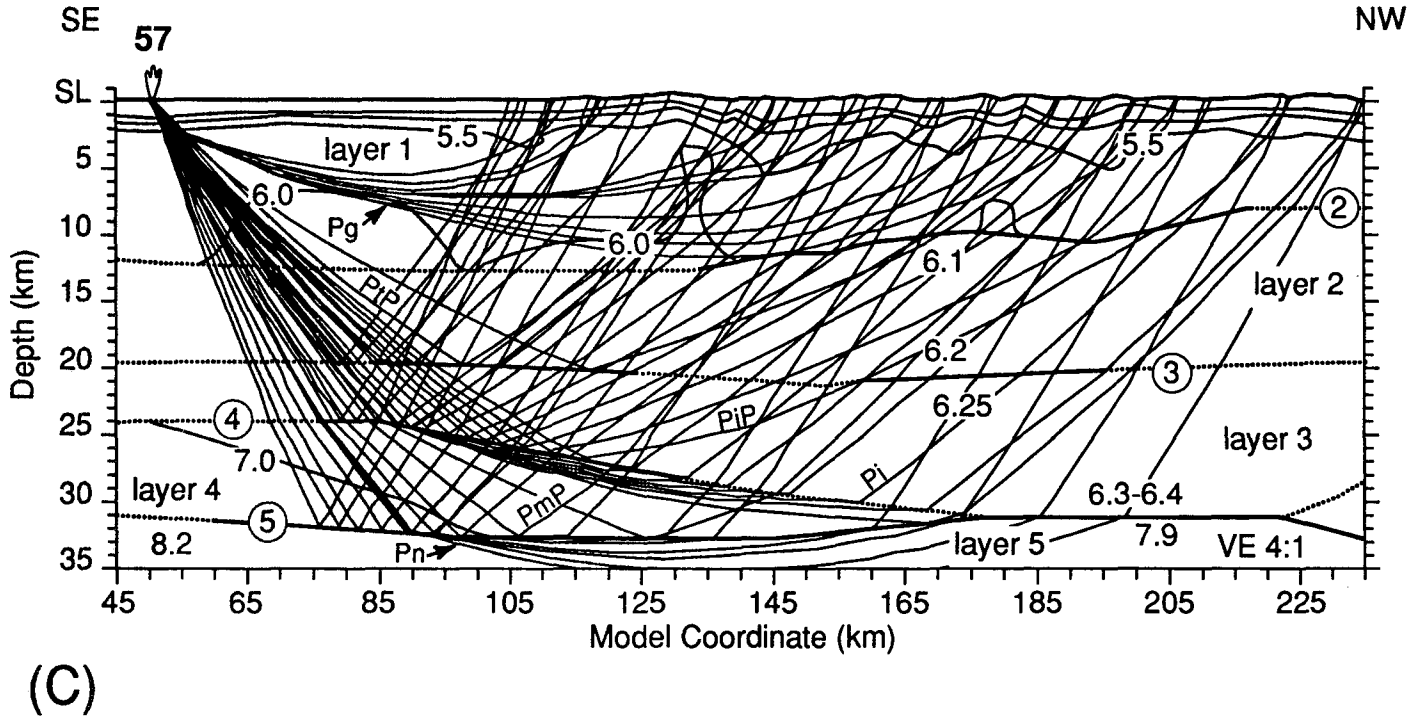

Figure 8. (*Continued*).

rocks along the contact. Tertiary granitic rocks intrude these terranes locally and may offer an alternate explanation for this region of higher velocity.

The central domain exhibits lower average velocities and weaker velocity gradients than the northern and southern domains. This region underlies the Manley, Livengood, and Mount Schwatka terranes. The nature of the southern boundary of the Manley terrane has been debated by several workers and is crucial to the various tectonic models proposed for the region. Geometries for the Manley terrane include: (1) a shallow, basin-like structure truncated to the south by a high-angle fault (Weber, 1990); (2) a shallow basin overthrust from the south by the Yukon-Tanana terrane and thrust over the Livengood terrane to the north (Dover, 1990; Grantz and others, 1991); and (3) a deep basin overthrust from both the north and south by the Yukon-Tanana and Livengood/Ruby terranes, respectively (Coney and Jones, 1985; Jones and others, 1986). Whether the Manley terrane (including KJs, Fig. 10) extends southward beneath the mapped trace of the Beaver Creek fault, which would indicate a southward dip for the fault, is addressed by these refraction data. The velocity model suggests that the Beaver Creek fault either is a near-vertical fault or overlies a buried vertical fault (as suggested by Weber, 1989, personal commun.; 1990), and that this contact bounds the lower-velocity rocks of the Manley terrane. Along the profile, the northwestern boundary of the Mount Schwatka terrane is the Victoria Creek fault. Our data suggest that the Victoria Creek fault has an apparent northward dip (see above). The above observations imply that the Manley, Livengood, and Mount Schwatka terranes are bounded south by a vertical fault and north by a northward-dipping fault. The boundary between the Manley and Livengood terranes corresponds to a clear velocity anomaly (165–175 km) that is confined to the upper ~3–4 km of crust. However, the data do not have the resolution necessary to constrain the dip of this boundary.

The northernmost domain, north of the Victoria Creek fault, is less well constrained by our data. This domain exhibits strong lateral and vertical velocity gradients that might be expected from the Tozitna terrane composed of sedimentary rocks with voluminous mafic units. The base of the Tozitna terrane is interpreted to correspond with the strong PcP reflector, interface 2, at 8–10 km depth (see below). The Tozitna fault, interpreted along a prominent topographic lineament within the Tozitna terrane, corresponds to a slight velocity high at approximately model coordinate 220–225 km. Our profile, however, does not have the necessary shot and receiver coverage to elaborate on the geometry of the Tozitna fault.

Undercutting the central, northern, and part of the southern upper-crustal domains is the PcP reflector, interface 2. The difficulty we had modeling a significant change in velocity across interface 2 suggests that this reflector is a reflective zone within a more uniform velocity field. Beneath the northern domain, two possible explanations for this reflector are a mafic sill or the fault contact between the Tozitna and Ruby terranes. Mafic sills are observed in outcrop in the igneous section of the Rampart group (Cady, 1987) north of our profile. If interface 2 is a mafic sill, our data indicate that this feature extends beneath the Victoria Creek fault and the Manley/Livengood/Mount Schwatka terranes; however, the northern low-velocity anomaly in our model and the associated aeromagnetic discontinuity (Cady, 1991) would suggest that the igneous section of the Rampart group does not extend this far south. Our preferred interpretation for interface 2 is the fault contact between the Tozitna and Ruby terranes. Fountain and others (1984) have demonstrated that mylonitic shear zones can produce significant reflections from within an otherwise homogeneous region. Several authors have suggested that the Tozitna terrane was thrust over the Ruby terrane during a phase of continent-ocean collision (Moore and Murphy, 1989; Patton and others, 1989; Dover, 1990; Grantz and others, 1991). Thus, our data tentatively suggest that the basal contact of the Tozitna terrane lies at ~8–10 km depth beneath the profile and dips gently southeastward (Fig. 7B).

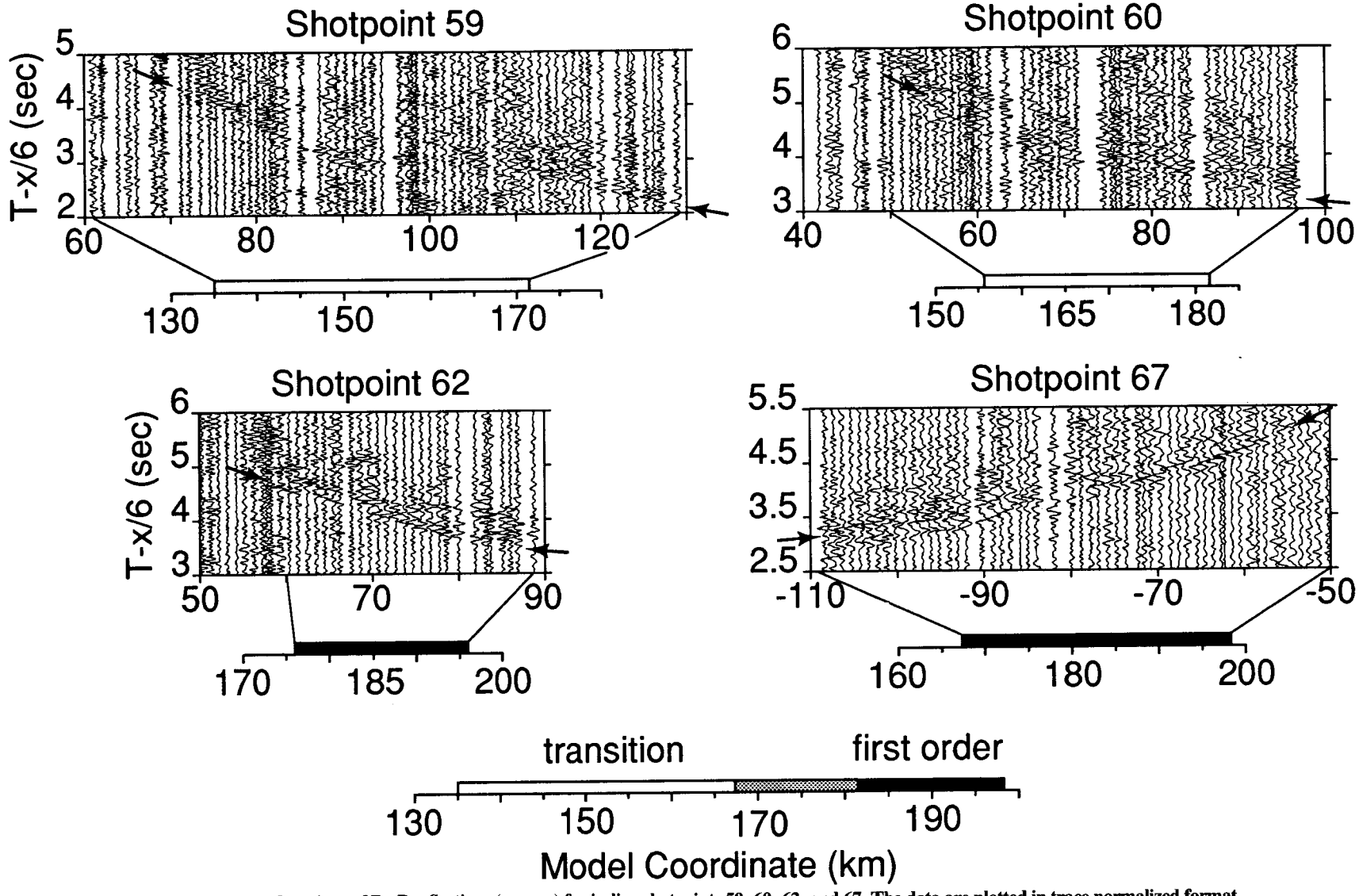

Figure 9. Record sections of PmP reflections (arrows) for in-line shotpoints 59, 60, 62, and 67. The data are plotted in trace normalized format. The scales beneath each plot show, in model coordinates, the bottoming points of the PmP reflection as determined from the final velocity model. The open bar denotes a poorly defined reflection, and the solid bar denotes a clear, strong reflection. At the bottom of the plot, bottoming points for each of the 4 shotpoints have been overlain; the gray region denotes an overlap of the open and solid bars.

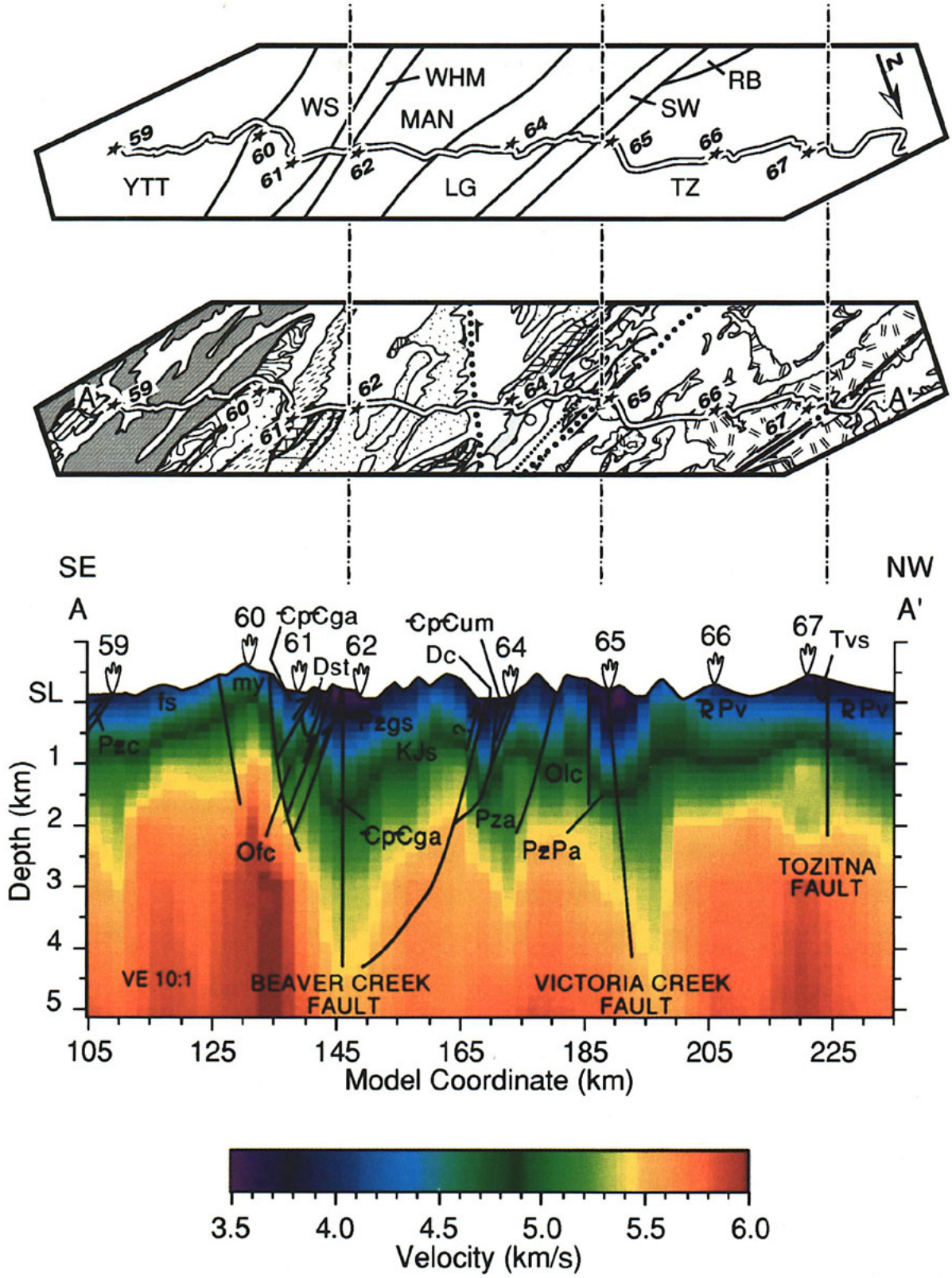

Figure 10. The inverse velocity model with a geologic cross-section overlay and a map view of the terranes (top) and geologic units (middle) crossed by the Fairbanks North profile. Strong correlations between observed geologic structural trends and the compressional-wave velocity structure are evident. The shotpoints are denoted by the numbered symbols. Geologic symbols are as follows: pЄf, Fairbanks schist unit; pЄg, Wickersham unit, basal grit subunit; ЄpЄga, Wickersham unit, maroon and green slate subunit; ЄpЄum, mafic and ultramafic complex; Pzc, Chatanika unit; Olc, Livengood Dome Chert; Dst, Tolovana Limestone; Dc, Cascaden Ridge unit; Pzgs, Globe unit; RPv, Rampart group; KJs, Wilbur Creek unit. See caption of Figure 1 for terrane abbreviations and Figure 2 for geologic units.

The apparent continuity of the PcP reflector from north to south beneath the profile (Fig. 3) may or may not be real. Small offsets (≤1 km) along this interface cannot be resolved by our data, but the data do indicate ≥1 km relief on this interface (Fig. 3A). Several interpretations are possible: (1) interface 2 represents a single thrust fault along which the terranes caught between the Yukon-Tanana and Ruby terranes (WS, WHM, LG, MAN, MNK, SW, TZ) were emplaced; (2) interface 2 represents a mid-crustal detachment associated with transformation of the Tintina fault dextral motion to compression in this region; or (3) interface 2 represents two or three separate thrust faults brought together (at ~10 km depth) by lateral offsets along the Tintina fault system. The rocks above this interface have velocities expected for the mafic volcanic and volcaniclastic rocks of the Tozitna terrane. Beneath this interface the velocity structure is fairly homogeneous and has modeled velocities in keeping with laboratory-measured velocities for the central portion of the Yukon-Tanana terrane (Beaudoin and others, 1992); the Yukon-Tanana and Ruby terranes are lithologically similar and should exhibit similar velocities.

Middle to Lower Crust. Several lines of evidence suggest that the middle to lower crust beneath the profile consists of at least two crustal domains. This evidence includes the strong lateral low-velocity anomalies in the upper crust and the laterally variable character of PtP, PiP, and PmP. We have interpreted the two steeply dipping, upper-crustal, low-velocity anomalies as faults. The fault associated with the northern low-velocity anomaly is interpreted to penetrate the middle and lower crust. In contrast, the fault associated with the southern upper-crustal, low-velocity anomaly can either be confined to the upper crust or extend into the middle and lower crust. These further interpretations are based on the observation that, for faults defined by velocity structure, a shallow fault will produce a downward tapering of the velocity field contours with depth (the V-like structure at ~145 km in Fig. 3), and a deep-penetrating fault will produce a broadening of the velocity field contours with depth (the broad region around model coordinate 195 km in Fig. 3) (W. J. Lutter, unpub. data). An alternate interpretation for the fault associated with the southern low-velocity anomaly is that it juxtaposes similar velocities at depths >10 km and is, therefore, not imaged. In addition to being expressed in the velocity field, the northern low-velocity anomaly overlies a break in slope of interface 2 (Fig. 3A), suggesting that its associated fault continues to mid-crustal depths. The lack of strong lateral velocity variations beneath interface 2 is due, in part, to the resolution of this study. Support for the continuation of at least one of these interpreted upper-crustal faults into the middle crust is provided by lower crustal reflections.

Although the middle to lower crust becomes largely homogeneous in velocity, variability in reflection character for arrivals PtP, PiP, and PmP suggest differences in middle and lower crust from south to north. Interface 3 (PtP) marks the top of a zone of increased lower-crustal reflectivity, observed along the profile, which is most evident from the southern off-end shotpoints. The PtP reflector, interface 3, is modeled in two segments, between model coordinates 85 and 125 km and between model coordinates 155 and 195 km (Fig. 3). This reflection suggests at least two divisions of the middle crust. Interface 4 and layer 4 (PiP and Pi) are present south of model coordinate 175 km, absent between model coordinates 175 and 220 km, and present north of model coordinate 220 km. The presence of layer 4 is directly correlated with the variable reflection character of PmP, from discontinuous and scattered from regions where layer 4 is present to sharp and continuous from regions where layer 4 is absent. These two phases, PiP and PmP, suggest that the lower crust beneath the profile may be divided into three domains.

Our observations suggest that at least two middle- to lower-crustal domains abut at depth and that the Moho has only minor topography between them. The lack of significant Moho topography does not preclude distinct domains of lower crust, because the Moho may be younger than the tectonic structures separating these domains. Reequilibration of the Moho during thermal events (for example, Meissner and others, 1987) could account for a young Moho, and the widespread presence of Tertiary plutons provide evidence for a young thermal event. The broken appearance of PmP for the southern shotpoints can be produced in at least two ways: (1) incoherent reflections from short-wavelength topography on the Moho (Mereu, 1990) or (2) destructive interference of the wavefield within the basal crustal layer (Beaudoin and others, 1992). Layering in the basal crustal layer sufficient to produce destructive interference of the wavefield could be produced by igneous, metamorphic, or ductile processes.

Strands of the Tintina Fault

The Tintina fault has been interpreted to either continue southwestward through our study area (Dover, 1990; Weber, 1990) or terminate in the region between the Ruby and Yukon-Tanana terranes (Churkin and others, 1982; Coney and Jones, 1985). Workers who argue for a southwestward continuation of the Tintina fault through our study area propose two basic groups of models: models that rely largely on strike-slip, orogen-parallel terrane displacements, and models that rely largely on closure of an ancient oceanic basin as well as strike slip.

F. R. Weber (1989 and 1990 written commun.) postulates that three major splays of the Tintina fault divide this region into three blocks: (1) A southern block (Northern Yukon-Tanana, Wickersham, and White Mountains terranes) is bounded on the northwest by the Hot Springs strand, which lies at depth in the footwall beneath the Beaver Creek thrust. (2) A central block (Manley, Livengood, and Mount Schwatka terranes) lies between the Hot Springs strand and the Victoria Creek strand. (3) A Northern block (Tozitna terrane) occurs between the Victoria Creek and the Tozitna strand. Weber suggests that the cessation of movement along strands of the Tintina fault becomes younger to the northwest. The present-day configuration of these Tintina splays was shaped by the opening of the Arctic basin and the resultant counterclockwise rotation of western Alaska; with this rotation, younger splays of the Tintina fault became unfavorably oriented for continued dextral slip and, hence, new splays formed progressively northward. According to this interpretation, the terranes in this region were transported to their current locations along the Tintina fault system from original positions in the Canadian Cordillera by Cretaceous and earlier(?) right-slip transform displacement. Following emplacement by strike slip and rotation, this region underwent shortening and thrust faulting in response to continued dextral movement along the Tintina fault.

Dover (1990) interprets this region as a continental fold-and-thrust belt rather than a zone of terrane collision and suturing because of the absence of tectonic mélange, relict accretionary prism, or other evidence of suturing. Instead he proposes that a system of thrust-bound sequences characterize this region. These sequences were derived from the North American continent and later dispersed by right-slip faulting across east-central Alaska from original positions in the Canadian Cordillera. In the study area, Dover shows two strands of the Tintina fault, the Tozitna and the Victoria Creek faults. The Victoria Creek fault connects the Kaltag fault with the Tintina fault and in this interpretation, no southern splay of the Tintina fault exists. Thus, Dover (1990) suggests that con-

tractional deformation preceded translation, whereas Weber (1990) suggests that contractional deformation accompanied and followed translational displacement.

Unlike the right-slip models of Weber (1990) and Dover (1990), Churkin and others (1982), Coney and Jones (1985), and Jones and others (1986) suggested that this region formed by the accretion of exotic terranes during the closure of an ancient oceanic basin. In these interpretations, the Yukon-Tanana terrane accreted south of most of the smaller terranes and was transported along the dextral Tintina fault, later colliding with the small terranes to the north along northwest-vergent faults (Churkin and others, 1982; Coney and Jones, 1985). These interpretations differ from those of Weber (1990) and Dover (1990) on several points, most notably whether the Tintina fault is a continuous feature through this region (Dover, 1990; Weber, 1990) that possibly connects with the Kaltag fault (Dover, 1990) or whether the Tintina fault terminates in this region of compressional structures (Churkin and others, 1982; Coney and Jones, 1985).

Our seismic data imply that at least one of the two interpreted, steeply dipping faults cut the entire crust, suggesting that an intracontinental transform fault does pass through our study area. Because its seismic expression is limited to the upper crust, we cannot determine whether the southern vertical low-velocity anomaly (~145 km) penetrates to the base of the crust. Our data only suggest that this discontinuity is a shallow fault, perhaps even a conjugate strike-slip fault to the Denali and Tintina fault system as observed to the south (Page and others, 1989). The data, however, also allow this discontinuity to be a more deeply penetrating structure with no associated velocity expression. The seismic data suggest that the northern low-velocity anomaly (~195 km), which we interpret as the expression of the Victoria Creek fault, extends deeper than 10 km (see above). Based on the geometry of layer 4 (Fig. 3) and the variable nature of the Moho reflection (Fig. 9), this discontinuity may extend to the base of the crust. Although the shallow-dipping reflector (interface 2) associated with PcP crosses the interpreted Victoria Creek fault, a well-constrained break in geometry occurs at this point (~195 km), supporting the continuation of the Victoria Creek fault into the middle and lower crust. If the southern (≤195 km) and northern (≥195 km) segments of interface 2, on either side of the Victoria Creek fault, share a common origin, little apparent vertical movement has occurred across the Victoria Creek fault.

The seismic data alone cannot determine whether the interpreted crustal cutting fault, the Victoria Creek, defines the Tintina fault zone. To facilitate our interpretation, we combine our seismic data with existing geologic interpretations. The interpretations by Dover (1990) and Weber (1990) show the Victoria Creek fault as a strand of the Tintina fault system. Price and Carmichael (1986) interpreted the Tintina fault as an intracontinental transform fault, indicating that it should cut the entire crust, consistent with interpretations that the Victoria Creek fault cuts the entire crust and represents a strand of the Tintina fault. Structural similarities between our velocity model and the Tintina fault zone (Roddick, 1967; Foster, 1983), and the model proposed by Weber (1990) support an interpretation whereby at least one strand of the Tintina fault cuts through our study area. We therefore interpret our model as in-

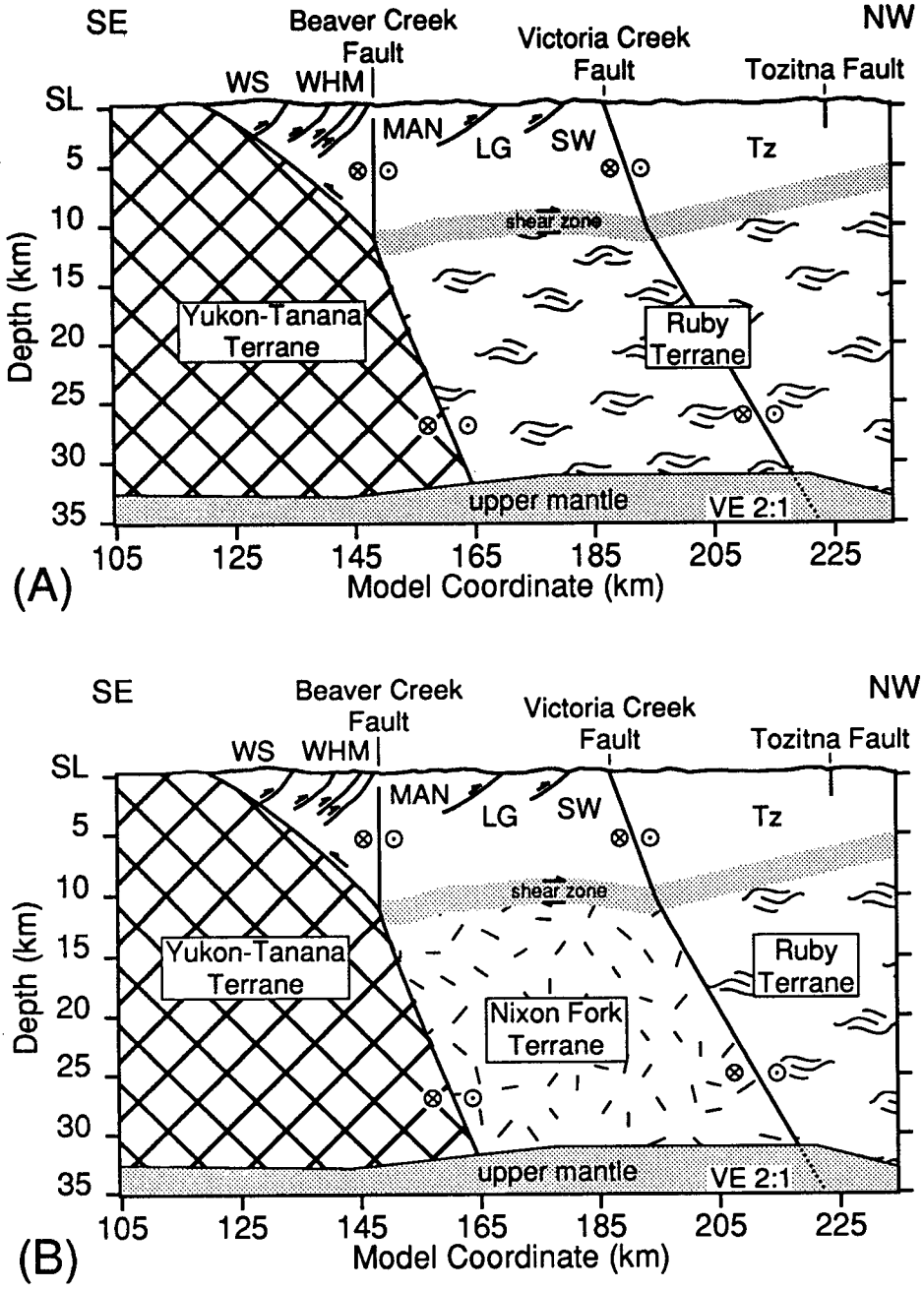

Figure 11. Two interpretive cross sections of the Fairbanks North velocity model. (A) The lower crust is divided into two domains: a southern domain consisting of the Yukon-Tanana terrane, and a northern domain consisting of the Ruby terrane. (B) The lower crust is divided into three domains: a southern domain consisting of the Yukon-Tanana terrane, a central domain consisting of the Nixon Fork terrane(?), and a northern domain consisting of the Ruby terrane. See caption of Figure 1 for terrane abbreviations.

dicating that the Victoria Creek fault represents a northwestward extension of the Tintina fault. Furthermore, our seismic data reveal a near-vertical fault, either the Beaver Creek or a buried fault, which supports the existence of a southern strand of the Tintina fault beneath our profile (Weber, 1990; Weber and others, 1992).

Interpretation of the Middle and Lower Crust

Our data suggest a fundamental difference between the middle to lower crust in the southern and northern parts of the profile. The reflection character from shotpoint 57 is similar to that presented by Beaudoin and others (1992). The velocity structure (including layer 4) associated with this reflection character does not extend north of approximately model coordinate 175 without disruption. This observation, coupled with observations that indicate the presence of at least two lower-crustal domains beneath the profile, suggest that the northern limit of the Yukon-Tanana terrane lies beneath the Fairbanks North profile. A plausible location for the northern boundary of the Yukon-Tanana terrane is at the strong, vertical, low-velocity anomaly in the upper crust at model coordinate 145 km and at greater depth along a northwest-dipping boundary connecting to the change in reflection character of the Moho and the pinch-out of layer 4 at model coordinate 175 km (Fig. 11A). A correlative interpretation is that the Yukon-Tanana and Ruby terranes underlie the seismic profile and join along this boundary. The lack of velocity contrast to suggest such a contact at depth is not surprising, because the Yukon-Tanana and the Ruby terranes have similar lithologic composition (Dover, 1990).

An alternate interpretation emphasizes the division of the lower crust into three domains (Fig. 11B). The southern domain encompasses the Yukon-Tanana terrane lower crust and is bounded on the northwest by the projection of the upper-crustal, vertical, low-velocity anomaly at ~145 km into the lower crust. This southern domain has a lower crust characterized by a basal crustal layer (layer 4) and a PmP reflection that is not well defined. The central domain lies between the southern domain and the Victoria Creek fault, lacks a basal crustal layer, but has a strong PmP reflection. The northernmost domain seismically resembles the southern domain. This interpretation allows the lower crust beneath the Manley, Livengood, and Mount Schwatka terranes to be entirely different from that to the north and south. Grantz and others (1991) have postulated that these terranes are underlain by the large Nixon Fork terrane, which may plunge eastward from its area of exposure to the west (Fig. 1). The Nixon Fork terrane consists of metamorphic rocks generally similar in composition to those of the Yukon-Tanana and Ruby terranes. The similarity in composition would suggest similar velocities and be consistent with the velocity model. In this interpretation, the two steeply dipping, upper-crustal faults continue to at least the base of the crust, linking the upper and lower crustal domains. The appeal of this interpretation is that the existence of layer 4 is directly correlated with different lower crustal units; a two-domain lower crust requires a 50-km-wide transition zone from the Yukon-Tanana terrane to Ruby terrane to account for the absence of layer 4 and the strong Moho reflection.

TECTONIC INTERPRETATION AND CONCLUSIONS

The TACT Fairbanks North profile provides new data that helps resolve some of the controversies and unanswered questions on the region between the Yukon-Tanana and Ruby terranes. Our data reveal a crustal velocity structure that is divided into three upper-crustal and at least two middle- to lower-crustal domains. The identification of these domains allows us to establish terrane geometries, speculate on the nature and locality of the Tintina fault zone, and finally, infer a tectonic history.

The upper-crustal domains correlate well with mapped surface geology. Within the southern domain, the Wickersham and White Mountains terranes are expressed by high-velocity, finger-like features in accordance with the exhumation of higher velocity rocks from the southeast. In the central domain, lower average velocities and the lack of strong vertical and lateral velocity gradients indicate a more homogeneous region. We interpret the corresponding Manley, Livengood, and Mount Schwatka terranes to be bound south by a near-vertical fault and north by a northward-dipping fault. The northern domain has a strong upper-crustal reflection that is interpreted as the shear interface between the Tozitna and Ruby terranes. The continuation of this interface beneath the central domain suggests that it may represent the detachment or basal thrust for thin-skinned tectonic amalgamation of the terranes caught between the Yukon-Tanana and Ruby terranes. The lower crust and Moho reflection exhibit differences from north to south that define at least two lower-crustal domains, interpreted as the Yukon-Tanana and Ruby terranes. However, whether a third, central domain at middle- to lower-crustal depths is distinct from the northern domain cannot be definitively established by these data. Finally, the crustal thickness between the northern and southern domains has only minor differences and is mapped at 31–34 km in depth.

Although surface geology exhibits compressional structures often associated with thrust faulting, the steep faults and lower crust are suggestive of a later period of strike-slip tectonics. We interpret these observations to indicate that after initial thin-skinned amalgamation of the various terranes, this region experienced thick-skinned tectonic reorganization via strike-slip faulting. This interpretation supports models that require at least one strand of the Tintina fault to exist in this important region of Alaska.

ACKNOWLEDGMENTS

We thank John Cady, Arthur Grantz, Robert Jachens, Jill McCarthy, Warren Nokleberg, and Robert Page for insightful reviews and suggestions that helped improve this manuscript. We gratefully acknowledge the assistance in our field work and initial data processing provided by Elizabeth Ambos, Patricia Berge, Robert Colburn, Charles Collum, George Corbin, Joseph Cotton, Ernst Flueh, Liz Green, Ronald Kaderabek, William Kohler, Robert Luzitano, Robert McClearn, Janice Murphy, Benjamin Page, David Reneau, Scott Schapper, Julie Shemeta, John Van Schaack, Dean Whitman, and Jeffrey Wilson. We thank especially Edward Criley, who supervised field operations. We are indebted to our Canadian colleagues Timothy Cote, Terry Neufeld, and Carl Spencer for graciously contributing twenty instruments to our experiments, operating the instruments, and reducing the data. We also thank our colleagues at the University of Alaska at Fairbanks, David Stone, John Davies, and Lorraine Wolf, who kindly allowed us to house our computer at their university.

APPENDIX 1.

This appendix contains trace normalized record sections (Figs. A1A–A1F) for shotpoints not discussed in detail within the text. Overlain on the record sections are calculated traveltimes derived from the final Fairbanks North velocity model. Refractions are represented by the closely spaced dotted lines, sub-critical reflections by the widely spaced dotted lines, and supercritical reflections by the dashed lines. Critical points are denoted by the solid circles. All record sections have been bandpass filtered from 1 to 12.5 Hz.

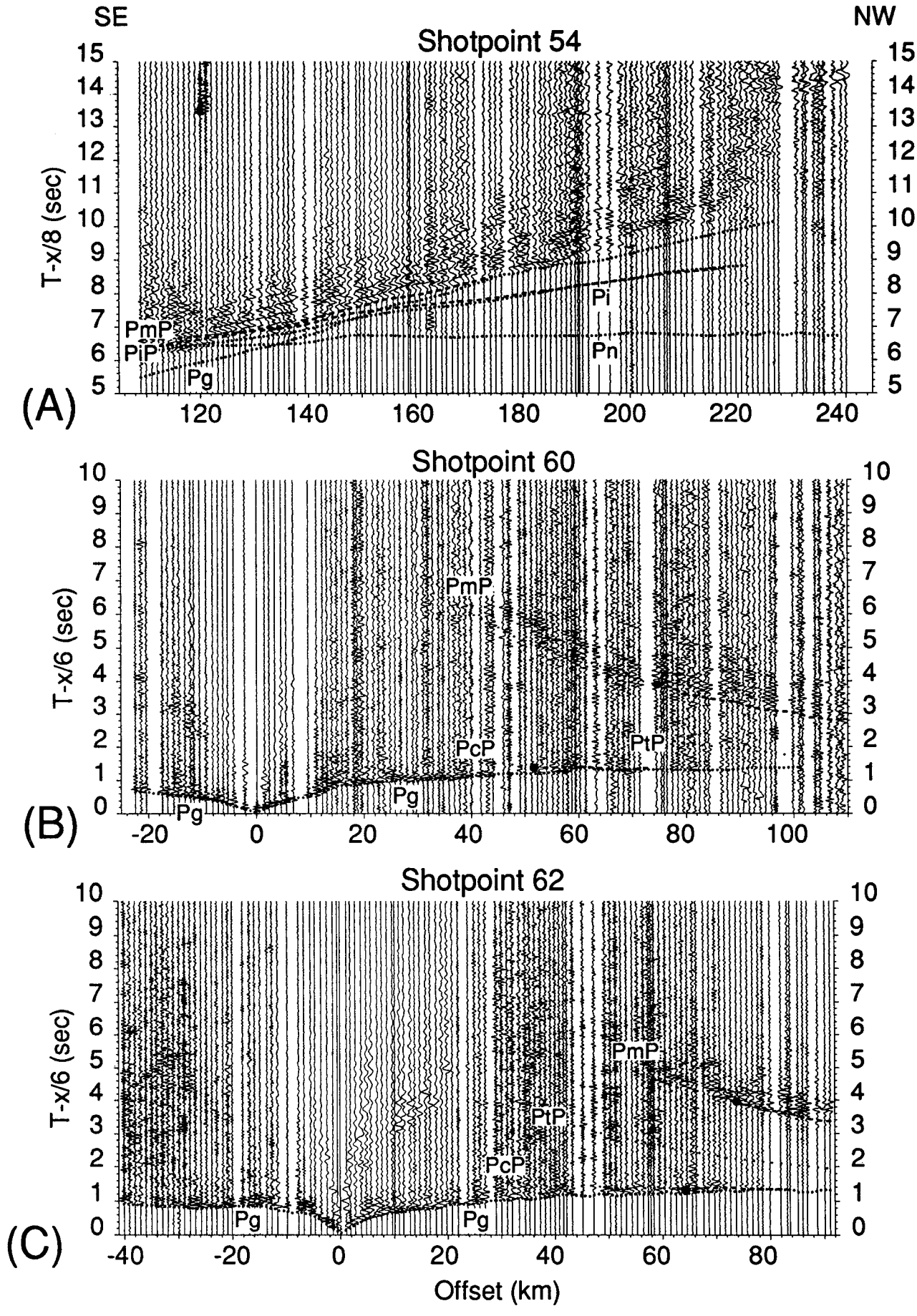

Figure A1. Trace normalized record sections for shotpoints not discussed in detail. (A) Record section for shotpoint 54, (B) shotpoint 60, (C) and shotpoint 62.

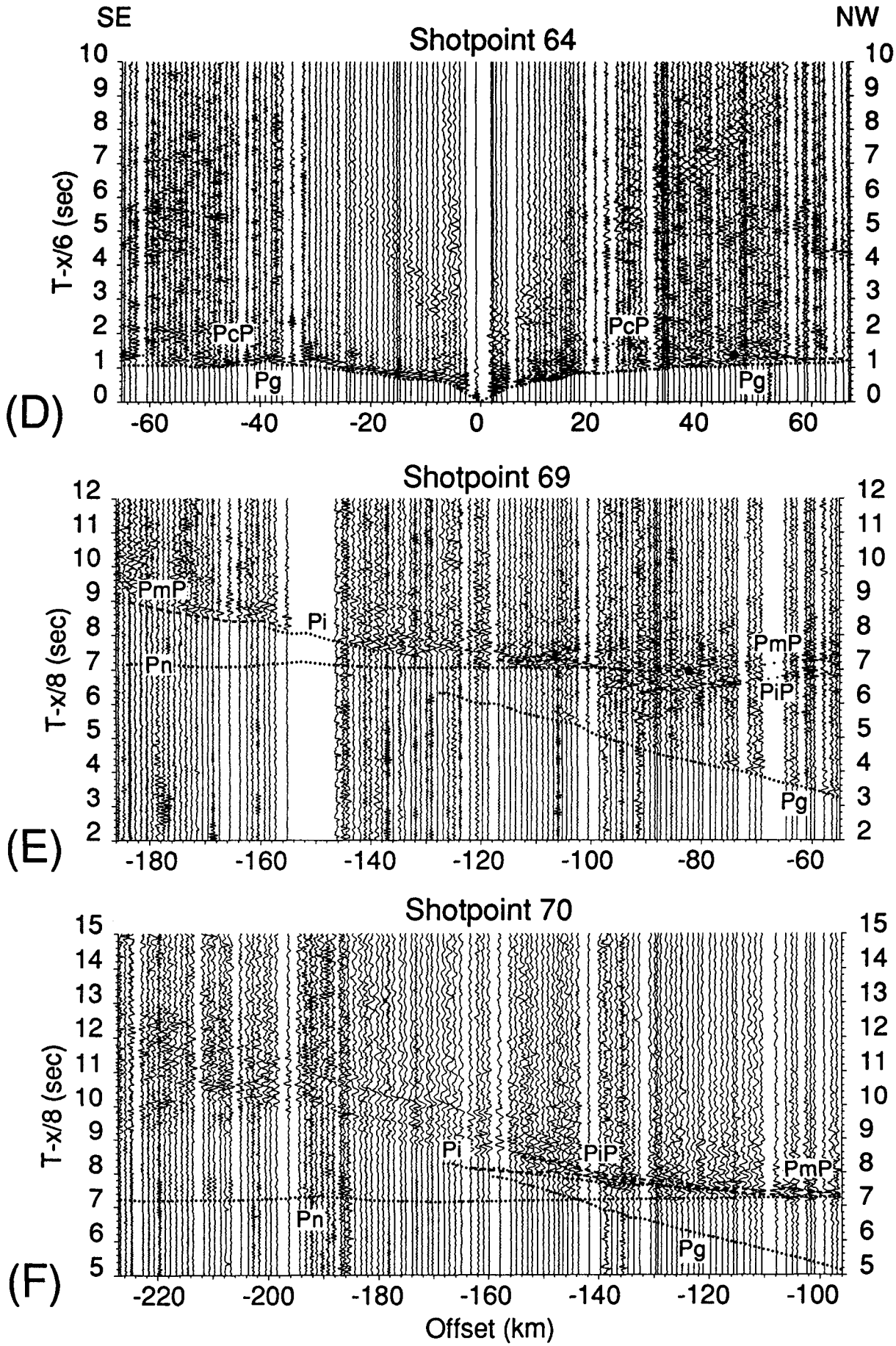

Figure A1. (*Continued*). (D) Record section for shotpoint 64, (E) shotpoint 69, and (F) shotpoint 70.

REFERENCES CITED

Arth, J. G., Zmuda, C. C., Foley, N. K., Criss, R. E., Patton, W. W., Jr., and Miller, T. P., 1989, Isotopic and trace element variations in the Ruby batholith, Alaska, and the nature of the deep crust beneath the Ruby and Angayucham terranes: Journal of Geophysical Research, v. 94, p. 15941–15955.

Beaudoin, B. C., 1992, Seismic investigations of the Earth's crust: Velocity structure and tectonics, Yukon-Tanana terrane, Alaska, and near surface effect on wave propagation, Ross ice shelf, Antarctica [Ph.D. thesis]: Stanford, California, Stanford University, 224 p.

Beaudoin, B. C., Perkins, G., and Fuis, G. S., 1989, Data report for the TACT 1987 seismic refraction survey: Alaska Range and Fairbanks South deployments: U.S. Geological Survey Open-File Report 89-321, 114 p.

Beaudoin, B. C., Fuis, G. S., Mooney, W. D., Nokleberg, W. J., and Christensen, N. I., 1992, Thin, low-velocity crust beneath the southern Yukon-Tanana terrane, east-central Alaska: Results from TACT refraction/wide-angle reflection data: Journal of Geophysical Research, v. 97, p. 1921–1942.

Blodgett, R. B., Wheeler, K. L., Rohr, D. M., Harris, A. G., and Weber, F. R., 1987, A Late Ordovician age reappraisal for the upper Fossil Creek Volcanics, and possible significance for glacio-eustasy, *in* Hamilton, T. D., and Galloway, J. P., eds., Geologic studies in Alaska by the U.S. Geological Survey during 1986: U.S. Geological Survey Circular 998, p. 54–58.

Brosgé, W. P., Lanphere, M. A., Reiser, H. N., and Chapman, R. M., 1969, Probable Permian age of the Rampart Group, central Alaska: U.S. Geological Survey Bulletin 1294-B, 18 p.

Cady, J. W., 1987, Preliminary geophysical interpretation of the oceanic terranes of interior Alaska: Evidence of thick crust of intermediate density, *in* Leitch, E. C., and Scheiber, E., eds., Terrane accretion and orogenic belts: American Geophysical Union Geodynamics Series, v. 19, p. 301–305.

Cady, J. W., 1991, Aeromagnetic map of Alaska from lat. 65°–68°N. long. 141°–162°W.: Color-shaded relief: U.S. Geological Survey Geophysical Investigations Map GP-992, scale 1:500,000.

Červený, V., Molotkov, I. A., and Pšenčík, I., 1977, Ray method in seismology: Prague, University of Karlova, 214 p.

Chapman, R. M., Weber, F. R., and Taber, B., 1971, Preliminary geologic map of the Livengood quadrangle, Alaska: U.S. Geological Survey Open-File Report 71-66, 2 sheets, scale 1:250,000.

Chapman, R. M., Weber, F. R., Churkin, M., Jr., and Carter, C., 1980, The Livengood Dome Chert, a new Ordovician formation in central Alaska and its relevance to displacement on the Tintina fault: U.S. Geological Survey Professional Paper 1126-F, p. F1–F13.

Churkin, M., Jr., Carter, C., and Trexler, J. H., Jr., 1980, Collision-deformed Paleozoic continental margin of Alaska—Foundation for microplate accretion: Geological Society of America Bulletin, v. 91, p. 648–654.

Churkin, M., Jr., Foster, H. L., Chapman, R. M., and Weber, F. R., 1982, Terranes and suture zones in east central Alaska: Journal of Geophysical Research, v. 87, p. 3718–3730.

Coney, P. J., and Jones, D. L., 1985, Accretion tectonics and crustal structure in Alaska: Tectonophysics, v. 119, p. 265–283.

Dover, J. H., 1990, Geology of east-central Alaska: U.S. Geological Survey Open-File Report 90-289, 91 p.

Foster, H. L., Laird, J., Keith, T. E. C., Cushing, G. W., and Menzie, W. D., 1983, Preliminary geologic map of the Circle quadrangle, Alaska: U.S. Geological Survey Open-File Report 83-170A, 32 p., scale 1:250,000.

Foster, H. L., Keith, T. E. C., and Menzie, W. D., 1987, Geology of east-central Alaska: U.S. Geological Survey Open-File Report 87-188.

Fountain, D. M., Hurich, C. A., and Smithson, S. B., 1984, Seismic reflectivity of mylonite zones in the crust: Geology, v. 12, p. 195–198.

Gabrielse, H., 1985, Major dextral transcurrent displacements along Northern Rocky Mountain Trench and related lineaments in north-central British Columbia: Geological Society of America Bulletin, v. 96, p. 1–14.

Gordey, S. P., 1981, Stratigraphy, structure and tectonic evolution of southern Pelly Mountains in the Indiago Lake area, Yukon Territory: Geological Survey of Canada Bulletin 318, 44 p.

Grantz, A., 1966, Strike-slip faults in Alaska: U.S. Geological Survey Open-File Report 267, 82 p.

Grantz, A., Moore, T. E., and Roeske, S. M., 1991, Continent-ocean transect A-3: Gulf of Alaska to Arctic Ocean: Boulder, Colorado, Geological Society of America, 72 p.

Jones, D. L., Silberling, N. J., and Coney, P. J., 1986, Collision tectonics in the Cordillera of western N. America: Examples from Alaska, *in* Coward, M. P., and Reis, A. C., eds., Collision tectonics: Geological Society Special Publication 19, p. 367–387.

Jones, D. L., Silberling, N. J., Coney, P. J., and Plafker, G., 1987, Lithotectonic terrane map of Alaska (west of the 141st Meridian): U.S. Geological Survey Miscellaneous Field Studies Map MF-1874-A, scale 1:2,500,000.

Loney, R. A., and Himmelberg, G. R., 1988, Ultramafic rocks of the Livengood terrane, *in* Galloway, J. P., and Hamilton, T. D., eds., Geologic studies in Alaska by the U.S. Geological Survey during 1987: U.S. Geological Survey Circular 1016, p. 68–70.

Luetgert, J. J., 1988, Users manual for RAY84/R83PLT: Interactive two-dimensional raytracing/synthetic seismogram package: U.S. Geological Survey Open-File Report 88-238.

Luetgert, J. J., 1992, Interactive seismic raytracing for the Macintosh™: U.S. Geological Survey Open-File Report 92-356.

Lutter, W. J., Nowack, R. L., and Braile, L. W., 1990, Seismic imaging of upper crustal structure using travel times from the PASSCAL Ouachita experiment: Journal of Geophysical Research, v. 95, p. 4621–4631.

Meissner, R., Wever, Th., and Flüh, E. R., 1987, The Moho in Europe—Implications for crustal development: Annales Geophysicae, v. 5, p. 357–364.

Mereu, R. F., 1990, The complexity of the crust from refraction/wide-angle reflection data: Pure and Applied Geophysics, v. 132, p. 269–288.

Mooney, W. D., and Prodehl, C., eds., 1984, Proceedings of the 1980 workshop of the International Association of Seismology and Physics of the Earth's Interior on the seismic modeling of laterally varying structures: Contributions based on data from the 1978 Saudi Arabian refraction profile: U.S. Geological Survey Circular 937, 158 p.

Moore, T. E., and Nokleberg, W. J., 1988, Stratigraphy, sedimentology, and structure of the Wickersham terrane in the Cache Mountain area, east-central Alaska, *in* Galloway, J. P., and Hamilton, T. D., eds., Geologic studies in Alaska by the U.S. Geological Survey during 1987: U.S. Geological Survey Circular 1016, p. 75–80.

Moore, T. E., and Murphy, J. M., 1989, Nature of the basal contact of the Tozitna terrane along the Dalton Highway, northeast Tanana quadrangle, Alaska, *in* Dover, J. H., and Galloway, J. P., eds., Geologic studies in Alaska by the U.S. Geological Survey, 1988: U.S. Geological Survey Bulletin B-1903, p. 46–53.

Nokleberg, W. J., Foster, H. L., and Aleinikoff, J. N., 1989, Geology of northern Copper River Basin, eastern Alaska Range, and southern Yukon-Tanana Basin, southern and east-central Alaska, *in* Nokleberg, W. J., and Fisher, M. A., eds., Alaskan geological and geophysical transect: Field Trip Guidebook T104: Washington, D.C., American Geophysical Union, p. 34–63.

Nowack, R. L., and Lutter, W. J., 1988, Linearized rays, amplitude and inversion: Pure and Applied Geophysics, v. 128, p. 401–421.

Page, R. A., Plafker, G., Davies, J. N., and Pulpan, H., 1989, Block rotation and seismicity in east-central Alaska [abs.]: Eos (Transactions, American Geophysical Union), v. 70, p. 1337.

Patton, W. W., Jr., and Box, S. E., 1989, Tectonic setting of the Yukon-Koyukuk basin and its borderlands, western Alaska: Journal of Geophysical Research, v. 94, p. 15807–15820.

Patton, W. W., Jr., Box, S. E., Moll-Stallcup, E. J., and Miller, T. P., 1989, Geology of west-central Alaska: U.S. Geological Survey Open-File Report 89-554, 41 p.

Price, R. A., and Carmichael, D. M., 1986, Geometric test for Late Cretaceous–Paleogene intracontinental transform faulting in the Canadian Cordillera: Geology, v. 14, p. 468–471.

Roddick, J. A., 1967, Tintina trench: Journal of Geology, v. 75, p. 23–33.

Tempelman-Kluit, D. J., 1976, The Yukon crystalline terrane: Enigma in the Canadian Cordillera: Geological Society of America Bulletin, v. 87, p. 1343–1357.

Weber, F., Foster, H. L., Keith, T. E. C., and Dusel-Bacon, C., 1978, Preliminary geologic map of the Big Delta quadrangle, Alaska: U.S. Geological Survey Open-File Report 78-529A, scale 1:250,000.

Weber, F., Smith, T. E., Hall, M. H., and Forbes, R. B., 1985, Geologic guide to the Fairbanks-Livengood area, east-central Alaska: Anchorage, Alaska Geological Society, 45 p.

Weber, F., 1990, Correlations across the western part of the Tintina fault system and their implications for displacement history [abs.]: Geological Association of Canada Program with Abstracts, v. 15, p. A138.

Weber, F. R., 1989, Geology between Fairbanks and the Yukon River, east-central Alaska, *in* Nokleberg, W. J., and Fisher, M. A., eds., Alaskan geological and geophysical transect: Field Trip Guidebook T104: Washington, D.C., American Geophysical Union, p. 84–95.

Weber, F. R., Wheeler, K. L., Rinehart, C. D., Chapman, R. M., and Blodgett, R. B., 1992, Geologic map of the Livengood quadrangle, Alaska, U.S. Geological Survey Open-File Report 92-562, scale 1:250,000.

Wheeler, K. L., Forbes, R. B., Weber, F. R., and Rinehart, C. D., 1987, Lithostratigraphy, petrology, and geochemistry of the Ordovician Fossil Creek Volcanics, White Mountains, east-central Alaska, *in* Hamilton, T. D., and Galloway, J. P., eds., Geologic studies in Alaska by the U.S. Geological Survey during 1986: U.S. Geological Survey Circular 998, p. 70–73.

MANUSCRIPT RECEIVED BY THE SOCIETY JANUARY 25, 1993
REVISED MANUSCRIPT RECEIVED JANUARY 28, 1994
MANUSCRIPT ACCEPTED FEBRUARY 1, 1994

Printed in U.S.A.